RSC Advances

PAPER

View Article Online
View Journal | View Issue

Cite this: *RSC Adv.*, 2023, **13**, 33080

Novel 2-substituted-quinoxaline analogs with potential antiproliferative activity against breast cancer: insights into cell cycle arrest, topoisomerase II, and EGFR activity†

Manar G. Salem,[a] Sara A. Abu El-ata,[b] Elsherbiny H. Elsayed,[b] Suraj N. Mali,[c] Hussah Abdullah Alshwyeh,[de] Ghassan Almaimani,[f] Riyad A. Almaimani,[g] Hussain A. Almasmoum,[h] Najla Altwaijry,[i] Ebtesam Al-Olayan,[j] Essa M. Saied *[kl] and Mohamed F. Youssef *[m]

Breast cancer is a global health concern, with increasing disease burden and disparities in access to healthcare. Late diagnosis and limited treatment options in underserved areas contribute to poor outcomes. In response to this challenge, we developed a novel family of 2-substituted-quinoxaline analogues, combining coumarin and quinoxaline scaffolds known for their anticancer properties. Through a versatile synthetic approach, we designed, synthesized, and characterized a set of 2-substituted quinoxaline derivatives. The antiproliferative activity of the synthesized compounds was assessed toward the MCF-7 breast cancer cells. Our investigations showed that the synthesized compounds exhibit considerable antiproliferative activity toward MCF-7 cells. Notably, compound **3b**, among examined compounds, displayed a superior inhibitory effect (IC_{50} = 1.85 ± 0.11 μM) toward the growth of MCF-7 cells compared to the conventional anticancer drug staurosporine (IC_{50} = 6.77 ± 0.41 μM) and showed minimal impact on normal cells (MCF-10A cell lines, IC_{50} = 33.7 ± 2.04 μM). Mechanistic studies revealed that compound **3b** induced cell cycle arrest at the G1 transition and triggered apoptosis in MCF-7 cells, as evidenced by increasing the percentage of cells arrested in the G2/M and pre-G1 phases utilizing flow cytometric analysis and Annexin V-FITC/PI analysis. Moreover, compound **3b** was found to substantially suppress topoisomerase enzyme activity in MCF-7 cells. Molecular modeling studies further supported the potential of compound **3b** as a therapeutic candidate by demonstrating significant binding affinity to the active sites of both topoisomerase II and EGFR proteins. Taken together, the presented 2-substituted-quinoxaline analogues, especially compound **3b**, show promise as potential candidates for the development of effective anti-breast cancer drugs.

Received 11th September 2023
Accepted 26th October 2023

DOI: 10.1039/d3ra06189b

rsc.li/rsc-advances

Introduction

Breast cancer is considered the second leading cause of death among women.[1] The significance of timely identification and intervention in breast cancer, before its metastasis, is of utmost importance, despite the ongoing discourse around the most effective approach to achieve this in recent times.[2] The annual incidence of common breast cancer has reached a staggering

[a]*Department of Pharmaceutical Organic Chemistry, Faculty of Pharmacy, Suez Canal University, Ismailia 41522, Egypt*
[b]*Department of Chemistry, Faculty of Science, Port Said University, Port Said, Egypt*
[c]*Department of Pharmaceutical Sciences and Technology, Birla Institute of Technology, Ranchi 835215, India*
[d]*Department of Biology, College of Science, Imam Abdulrahman Bin Faisal University, Dammam 31441, Saudi Arabia*
[e]*Basic & Applied Scientific Research Centre, Imam Abdulrahman Bin Faisal University, PO Box 1982, Dammam 31441, Saudi Arabia*
[f]*Department of Surgery, Faculty of Medicine, Umm Al-Qura University, Al Abdeyah, PO Box 7607, Makkah, Saudi Arabia*
[g]*Department of Biochemistry, Faculty of Medicine, Umm Al-Qura University, Al Abdeyah, PO Box 7607, Makkah, Saudi Arabia*
[h]*Department of Clinical Laboratory Sciences, Faculty of Applied Medical Sciences, Umm Al-Qura University, Al Abdeyah, PO Box 7607, Makkah, Saudi Arabia*
[i]*Department of Pharmaceutical Sciences, Princess Nourah Bint Abdulrahman University, PO Box 84428, Riyadh 11671, Saudi Arabia*
[j]*Department of Zoology, College of Science, King Saud University, Riyadh, Saudi Arabia*
[k]*Department of Chemistry (Biochemistry Division), Faculty of Science, Suez Canal University, Ismailia 41522, Egypt*
[l]*Institute for Chemistry, Humboldt Universität zu Berlin, Brook-Taylor-Str. 2, 12489 Berlin, Germany. E-mail: saiedess@hu-berlin.de*
[m]*Department of Chemistry (Organic Chemistry Division), Faculty of Science, Suez Canal University, Ismailia 41522, Egypt*

† Electronic supplementary information (ESI) available. See DOI: https://doi.org/10.1039/d3ra06189b

two million cases worldwide, accounting for a significant proportion of all cancer types.[3] It primarily originates in the lobules, which are responsible for producing milk, or the ducts that connect these lobules to the nipple.[4] Hormones, alcohol, obesity, and nulliparity, which have garnered public attention, have a very modest relative risk (<2%) for breast cancer.[5] Chemotherapy[6] has been widely recognized as the foremost efficacious therapeutic modality for the management of localized breast and liver malignancies as it impedes their molecular action by the initiation of apoptosis,[7] necrosis,[8] and autophagy, resulting in the death of cancer cells.[9] Besides chemotherapy, breast cancer patients have access to a wide range of treatment choices, including invasive and noninvasive biopsies, radiotherapy and molecular therapies.[10] However, most available medications lack specificity, which brings up problems like the well-documented side effects of cancer treatment[11] and the much more widespread phenomenon of multi-drug resistance.[12]

DNA topoisomerases are enzymes that play a crucial role in regulating DNA twists and folds.[13] Topoisomerases also play a vital role in preserving the structural integrity and stability of DNA,[14] which is essential for many complex biological processes like transcription, replication, and recombination[15] but can impede these activities and slow cell growth.[16] DNA damage,[17] slowed DNA replication,[18] unrepaired DNA strand breakage,[19] and cell death are all direct results of this blockade. Based on their ability to unwind both DNA strands at once, topoisomerases are categorized into two groups, topoisomerase I and topoisomerase II.[20] Topoisomerases I and II (Top 1 and Top 2 as they are more often known) are largely considered to be significant molecular targets for the development of anticancer medicines.[21] Irinotecan, topotecan, and camptothecin are well-known examples of topoisomerase I (Topo I) inhibitors.[22] On the other hand, etoposide, doxorubicin, and epirubicin are all examples of topoisomerase II (Topo II) inhibitors.[23] Due to its potential role as a therapeutic target and prognostic marker, Topo II has received a great deal of attention in the context of breast cancer.[24] Topo II exists in two forms, called Topo IIα and Topo IIβ.[25] DNA unwinding activity during replication is a hallmark of Topo IIα, and this protein has been considered to be a potential prognostic marker.[26] Topo IIα is often overexpressed in HER2-positive breast cancer cells and thus has been recognized as a potential pharmacological target for the treatment of breast cancer.[27,28]

Heterocycles are recognized as a profoundly auspicious category of compounds in the quest for innovative anticancer agents.[29] Quinoxaline has been identified as a prominent heterocyclic compound that has attracted considerable scientific attention.[30–32] The wide substitution of quinoxaline and their derivatives, together with their many biological features such as antiviral, anticancer, and antileishmanial activity, contribute to their promising prospects in the field of medicinal chemistry. They are increasingly acknowledged as a distinctive category of chemotherapeutic agents exhibiting notable efficacy against various types of tumors.[33] Quinoxaline-based compounds have shown significant anticancer efficacy by selectively inhibiting many cellular targets,[34] including topoisomerase,[35] VEGFR2,[36] telomerase,[37] farnesyltransferase,[38] tyrosine kinase,[39] and protein kinase CK-11 (Fig. 1). They hinder the proliferation and metastasis of breast cancer cells by targeting the PI3K/AKT/mTOR and MAPK/ERK pathways, as well as other proteins involved in angiogenesis. Additionally, quinoxaline derivatives impede the growth of ER-positive breast cancer cells by interfering with estrogen signaling at estrogen receptors.[40,41] Currently, there are several quinoxaline analogues which are under clinical investigations for their applicability as anti-tumor drugs, including CQS, GK13, tirapazamine, and *R*-(+)-XK469 (ref. 31 and 42–44) (Fig. 1).

The term "hybrid molecule" refers to the method used often in drug design to increase the potency, selectivity, and overall pharmacological characteristics of drugs by combining two distinct pharmacophores inside a single molecular scaffold.[45,46] This strategy takes use of the pharmacophores' distinct characteristics to provide a synergistic impact, which may increase efficacy against a target or illness.[47] Coumarins are heterocyclic polyphenolic chemicals found throughout plants.[48,49] Systematic research found 1300 secondary metabolite chemotypes in plants, microbes, and fungi.[50] The roots of *Ferulago campestris*,[51] *Murraya paniculata*[52] leaves, *Aegle marmelos*[53] fruits, and *tonka bean* seeds contain derivatives of coumarins with several biological functions. Synthetic coumarin-based heterocyclic analogues such azoles, sulfonyl, furan, and pyrazole have promise anticancer, antitumor, and anti-proliferative properties.[54,55] Natural coumarin-based compounds have demonstrated a potential anticancer activity by targeting several cellular targets including cycle arrest, angiogenesis, kinase activity, telomerase, and carbonic anhydrase.[54,56]

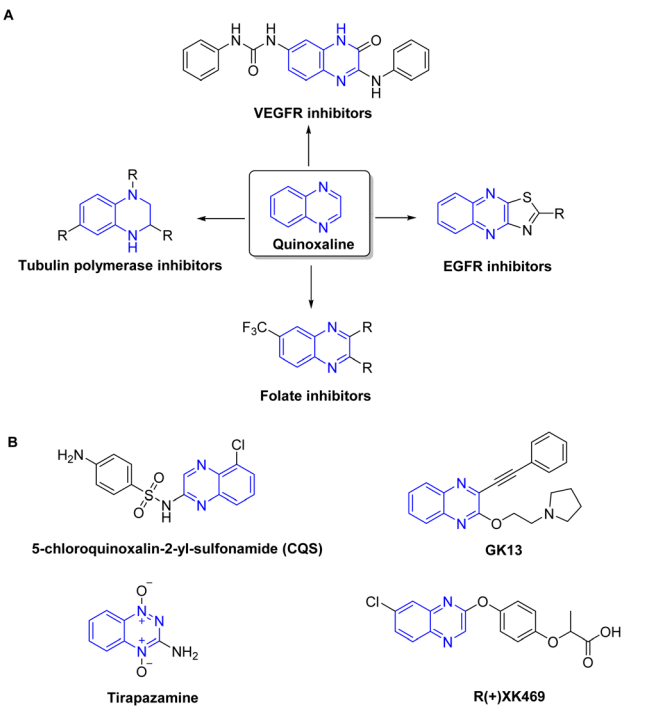

Fig. 1 Representative quinoxaline-based analogs with potent anti-tumor properties (A) and being examined in clinical trials (B).

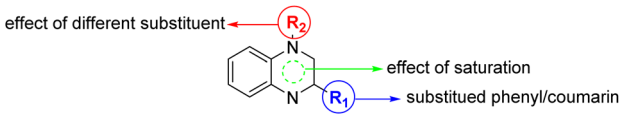

Fig. 2 Illustration of the structural features of designed hybridized 2-substituted-quinoxaline analogues bearing phenyl or coumarin moiety.

Considering the well-documented cytotoxic properties of coumarin- and quinoxaline-based compounds, our research hypothesis posits that the deliberate integration of these compounds into hybrid molecules may result in significant antitumor attributes worth exploring. Based on the above-mentioned facts, and our persistent interest in synthesizing bioactive compounds,[57–64] we aimed to design, synthesize, and characterized a new set of hybridized 2-substituted-quinoxaline derivatives bearing a phenyl/coumarin moiety (Fig. 2). The anti-proliferative activity of designed compound was assessed toward MCF-7 cells, and the mode of action was explored by investigating cell cycle arrest, and topoisomerase II activity. Finally, detailed computational analysis was performed utilizing molecular modelling and molecular simulation analysis to gain more insights to the mechanistic of this class of compounds.

Results and discussion

Chemistry

In the current research, we have developed a synthetic method for synthesizing new 2-substituted quinoxaline derivatives containing either a phenyl or an 8-methoxy-coumarin-3-yl group, as illustrated in Schemes 1 and 2, respectively. The synthesis started by the bromination of 5-bromo-2-hydroxy-acetophenone (**1a**) or 3-acetyl-8-methoxy-coumarin (**1b**) in the presence of glacial acetic acid to afford aryl bromomethyl ketones (**2a, b**), which are crucial intermediates in the synthesis of quinoxaline derivatives.[65,66] The reaction was conducted at a temperature of 60 °C with continuous stirring, following the established procedures described in the previous reports.[31] Compounds **2a** and **2b** were subjected to a condensation procedure employing *o*-phenylene diamine and molten sodium acetate in an ethanol solvent to furnish 2-(5-bromo-2-hydroxyphenyl)-3,4-dihydroquinoxaline (**3a**) and 2-(8-methoxy-coumarin-3yl)-3,4-dihydroquinoxaline (**3b**), with satisfactory yields of 56% and 61%, respectively. The nuclear magnetic resonance (^{1}H-NMR) spectra obtained for compounds **3a** and **3b** have revealed the presence of two distinct isomeric structures. The chemical confirmation of the structures of compounds **3a** and **3b** was achieved through a series of experimental procedures. Particularly, compounds **3a** and **3b**, were subjected to treatment with acetic anhydride under reflux conditions to afford 2-(2-acetoxy-5-bromo) phenyl quinoxaline (**4a**) and 2-(8-methoxy-coumarin-3-yl)-quinoxaline (**4b**) with yields of 73%, and 69%, respectively. The halogenation of compound **4a** was carried out by using bromine in glacial acetic acid, resulting in the formation of the corresponding 2-(5-bromo-8-methoxy-coumarin-3-yl) quinoxaline (**5**) with a yield of 82%.

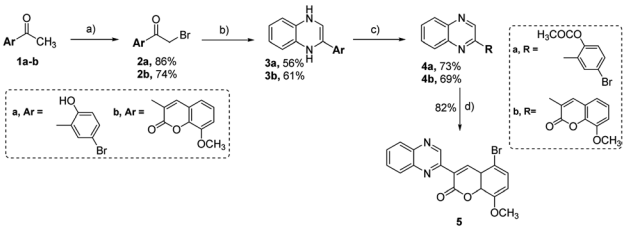

Scheme 1 Synthesis of 2-substituted-quinoxaline analogues bearing phenyl or coumarin moiety (**3a, b-5**). Regents and conditions: (a) Br_2, glacial AcOH, 60 °C-r. t., 12 h; (b) *o*-phenylene diamine, sodium acetate, EtOH, reflux, 12 h; (c) acetic anhydride, reflux, 14 h; (d) bromine, acetic acid, reflux, 8 h.

We expanded our investigation to explore the structural features of the 2-phenyl-substituted quinoxaline scaffold in greater depth. As shown in Scheme 2, 2-(5-bromo-2-hydroxyphenyl)-3,4-dihydroquinoxaline (**3a**) was further reacted with ethyl chloroacetate in the presence of triethyl amine to provide ethyl [3-(5-bromo-2-hydroxyphenyl)-1,4-dihydroquinoxalin-1-yl] acetate (**6**) with a yield of 68%. Further, compound **3a** was reacted with phenyl diazonium chloride in the presence of sodium hydroxide to afford 2-(5-bromo-3-phenylazo-2-hydroxyphenyl)-1,4-dihydroquinoxaline (**7**) with a yield of 71%. Finally, compound **7** was subjected to acetylation conditions using acetic anhydride under reflux to successfully furnish 2-(5-bromo-3-phenylazo-2-acetoxy) phenyl-quinoxaline-(**8**), with a yield of 86%.

Characterization of synthesized quinoxaline derivatives

The structural properties of all synthesized quinoxaline hybrids were thoroughly characterized using a variety of analytical

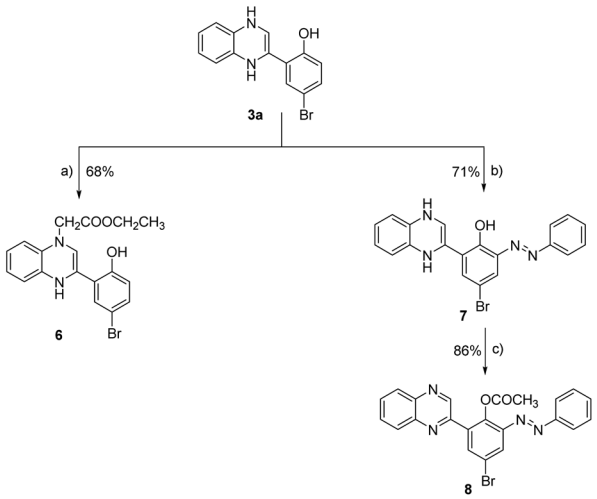

Scheme 2 Synthesis of 2-phenyl-quinoxaline analogues (**6–8**). Reagent and conditions: (a) ethyl chloroacetate, triethyl amine, DMF, reflux, 12 h; (b) phenyl diazonium chloride, 10% NaOH, 0–5 °C, 24 h; (c) acetic anhydride, reflux, 16 h.

techniques, such as nuclear magnetic resonance (NMR) spectroscopy and mass spectrometry. The nuclear magnetic resonance (^{1}H-NMR) spectra obtained for compounds **3a** and **3b** have provided valuable insights into the structural composition of these compounds, revealing the presence of two distinct isomers: 1,2-dihydroquinoxaline and 1,4-dihydroquinoxaline (Fig. S9†). This structural elucidation is visually represented in Scheme 1. The proton signal originating from the methylene (NCH_2) group of the isomeric 1,2-dihydroquinoxaline compound was observed at chemical shifts of approximately 4.40 and 4.02 ppm. Similarly, the ^{13}CNMR spectra displayed carbon signals corresponding to the methylene group at approximately 56.58 and 41.20 ppm. The proton signals originating from two NH groups in the isomeric form of 1,4-dihydroquinoxaline were observed within the chemical shift range of 9.60–9.72 ppm. The mass spectra analysis of dihydro quinoxaline derivatives (**3a** and **3b**) exhibited highly prominent molecular ion peaks at *m*/*z* 302 and 306, which corresponded to the molecular formulas $C_{14}H_{11}BrN_2O$ and $C_{18}H_{14}N_2O_3$, respectively. The mass spectrum analysis of compound **3a** revealed the presence of a molecular ion peak at *m*/*z* 302, which was identified as the base peak. In the instance of compound **3b**, it is noteworthy that the base peak manifested at *m*/*z* 304, which aligns with the molecular ion of compound **3b** following the elimination of hydrogen molecules (M^{+2}). The ^{1}H-NMR spectrum of compound **3a** exhibited singlet signals at a chemical shift of 2.22 ppm, which can be attributed to the presence of a methyl group associated with the acetyl group ($COCH_3$). Notably, there was an absence of any proton signal originating from the hydroxy group. The chemical compound known as azo methane (CH═N) within the quinoxaline ring exhibited a proton signal at a chemical shift of approximately 9.26 ppm. Furthermore, it is worth noting that the proton signals originating from aromatic rings were detected within the spectral region spanning from δ 7.37 to 8.19 ppm, manifesting as multiplet signals. The ^{13}C-NMR spectrum of compound **4a** exhibited two distinct carbon signals at chemical shifts of 169.48 and 21.19 ppm, respectively. These chemical shifts can be attributed to the presence of the acetoxy group ($OCOCH_3$) within the compound. The spectral analysis revealed the presence of carbon signals corresponding to quinoxaline and an aromatic ring, which manifested in the chemical shift regions of 149.51–119.31 ppm. It is noteworthy that the total number of carbon atoms in this system amounts to 14 carbons. The mass spectrum analysis of compound **4a** revealed a highly pronounced molecular ion peak at *m*/*z* 342, which aligns precisely with the molecular formula $C_{16}H_{11}BrN_2O_2$. The molecular ion peak observed at *m*/*z* 342 exhibited fragmentation, resulting in the emergence of a base peak at *m*/*z* 300. This base peak corresponds to the molecular ion peak of 2-(2-hydroxy-5-bromo) phenyl-quinoxaline radical cation. The fragmentation process involved the detachment of a ketene molecule (CH_2CO). The ^{1}H-NMR analysis of compound **4b** revealed the presence of three singlet signals at chemical shifts of 9.60, 8.89, and 3.97 ppm. These signals were attributed to the protons associated with the azomethine (CH═N) group in the quinoxaline ring, the H-4 proton in the coumarin ring, and the methoxy group (OCH_3), respectively. Furthermore, it is noteworthy that the protons associated with the quinoxaline and coumarin rings exhibited multiplet signals within the range of δ 6.56–8.16 ppm. Moreover, the structural verification of compound **4b** was substantiated through the analysis of its ^{13}C-NMR spectrum. Notably, the carbon signals observed at δ 56.67 and 56.16 ppm corresponded to the methoxy group (OCH_3) present in both stereo isomers of the compound. In addition, it is worth noting that the carbon signals originating from the quinoxaline and coumarin rings have been detected within the spectral region spanning from 159.84 to 114.34 ppm. The mass spectrum analysis of compound **4b** revealed the presence of a stable molecular ion peak at *m*/*z* 304. This peak corresponds to the molecular formula $C_{18}H_{12}N_2O_3$. The spectral analysis revealed the emergence of three distinct carbon signals at δ 168.79, 65.83, 61.38, and δ 14.47 ppm, which have been confidently attributed to the ethyl acetate fragment (NCH_2-$COOCH_2CH_3$). The ^{1}H-NMR spectrum analysis of compound **7** revealed the presence of four singlet signals at chemical shift values of 14.88, 12.19, 9.68, and 4.52 ppm. These signals can be attributed to the protons associated with the hydroxyl (OH), amino (NH), and *N*-methylene (NCH_2) functional groups within the compound. The multiplet signals observed in the region of approximately 6.47–8.19 ppm correspond to the proton signals (–CH═) originating from the aromatic and quinoxaline ring structures. The ^{13}C-NMR spectrum of compound **7** displayed carbon signals within the anticipated chemical shift range of 157.63–111.26 ppm. The ^{1}H-NMR spectrum analysis of compound **8** revealed the absence of proton signals at chemical shifts of approximately 14.88, 12.19, 9.68, and 4.52 ppm in the presence of compound **7**. Conversely, new proton signals emerged at chemical shifts of approximately 9.77, 9.24, 2.21, and 1.74 ppm, which can be attributed to the protons of the azomethine (CH═N) group in quinoxaline and the acetoxy ($OCOCH_3$) groups. These findings provide evidence for the existence of two stereoisomers in the compound under investigation. Moreover, the ^{13}C NMR spectrum of compound **8** exhibited the emergence of two distinct carbon signals, corresponding to two isomers, at chemical shifts of 174.63 and 169.41 parts per million (ppm). These shifts are in reference to the carbon atom within the acetyl group ($COCH_3$). Additionally, a separate carbon signal was observed at chemical shifts of 24.25 and 21.16 ppm, also referencing the carbon atom of the acetyl group. The mass spectrum analysis of compound **7** revealed the presence of a molecular ion peak at *m*/*z* 402, which exhibited a relatively low intensity. Conversely, the mass spectrum analysis of compound **8** indicated an unstable molecular ion peak. The fragmentation of compounds **7** and **8** resulted in the generation of a stable peak at *m*/*z* 221, which corresponds to the molecular ion of 2-(2-hydrophenyl) quinoxaline cation $[C_{14}H_9NO_2]^+$.

Assessment of cytotoxic activity against MCF-7 cells

We initially assessed the anti-proliferative activity of synthesized 2-substituted-quinoxaline derivatives (**3b**, **4a**, **4b**, **5**, **6**, and **7**) on the viability of two different cell lines: MCF-7, which

represents breast cancer cells, and MCF-10A, representing normal breast cells. To assess the anticancer potential of these compounds, we employed the 3-(4,5-dimethylthiazol-2-yl)-2,5-diphenyl tetrazolium bromide (MTT) colorimetric assay which is a widely utilized technique to evaluate cell viability and cytotoxicity. In our investigations, we incorporated staurosporine (STU) as a reference standard drug due to its well-established effectiveness as an anticancer agent. The MCF-7 and MCF-10A cell lines were subjected to different doses of synthesized quinoxaline derivatives, and the resulting cytotoxicity was evaluated in a dose-dependent manner (Fig. 3). Our results reveal that the developed 2-substituted quinoxaline analogues exhibit a broad range of anti-proliferative activity, spanning from moderate to highly potent. The evaluation of cytotoxic activity in 2-phenyl-substituted quinoxaline analogs (**3a**, **4a**, **6**, **7**, and **8**) highlighted essential structural characteristics that could be linked to the anti-proliferative properties of these compounds. As shown in Fig. 3, compound **3a** with quinoxaline scaffold substituted at position 2 with 5-bromo-2-hydroxy-phenyl moiety exhibited a considerable cytotoxic activity with IC_{50} of 12.74 μM. Acylation of the hydroxyl-group at the 2-postion of the phenyl moiety of compound **3a** afforded a compound with attenuated cytotoxic activity (**4a**, IC_{50} of 20.8 μM), suggesting the role of the hydroxyl-group on the anti-proliferative activity of the 2-phenyl substituted-quinoxaline scaffold. Similarly, alkylation of the quinoxaline scaffold at N_4-position with ethylacetate moiety significantly reduced the cytotoxic activity of the quinoxaline analogue (compound **6**, IC_{50} = 62.4 μM), indicating that the 1,4-quinoxaline ring play a substantial role in the observed anti-proliferative activity of this class. Interestingly, the addition of phenyl diazonium moiety at position-3 in the 2-phenyl-quinoxaline scaffold significantly improved the cytotoxic activity of the compound as indicated for compound 7 with IC_{50} of 8.6 μM. This finding indicates that the modification of 2-phenyl-quinoxaline can be extended for further investigations. Similar to compound **4a**, acylation of the hydroxyl group at position 2 in the phenyl moiety of compound 7 substantially reduced the anti-proliferative activity of compound (compound **8**, IC_{50} = 17.3 μM). These results further affirm the critical role of the OH-group in the activity of 2-phenyl-substituted quinoxaline scaffold. On the other hand, the evaluation of 2-(8-methoxy-coumarin-3-yl)-quinoxaline analogues (**3b**, **4b**, and **5**) revealed that these compounds possess a potential anti-proliferative activity. Our assessments indicated that compound **3b** with 2-(8-methoxy-coumarin-3-yl)-moiety display a substantial anti-proliferative activity with IC_{50} of 1.85 μM. The observed cytotoxic activity of compound **3b** was significantly attenuated upon conversion of quinoxaline moiety to 1,4-dihydroquinoxaline, as indicated in compound **4b** with IC_{50} of 4.08 μM. These results support the crucial role of the quinoxaline ring and further indicate that the two-NH groups play a significant role in the binding of this class of compounds toward the target protein(s). Finally, bromination of the 8-methoxy-coumarin moiety significantly impaired the anti-proliferative activity of the 2-(8-methoxy-coumarin)-quinoxaline scaffold (compound **5**, IC_{50} = 55.0 μM).

Among screened compounds, compound **3b** exhibited the most potent inhibitory activity toward the growth of MCF7 cells with IC_{50} value of 1.85 ± 0.11 μM (Fig. 4). To provide a contextual framework, we conducted a comparative analysis between the activity of compound **3b** and the anticancer drug staurosporine. STU demonstrated an IC_{50} value of 6.77 ± 0.41 μM on the proliferation MCF-7 cells. The observed difference in IC_{50} values suggests that compound **3b** is more effective in inhibiting the proliferation of MCF-7 cells compared to the reference drug STU. Encouraged by these findings, we redirected our research efforts towards a more comprehensive investigation of the anti-proliferative effects of compound **3b** on normal breast cells (MCF-10A). The evaluation of the selectivity of possible anticancer drugs is crucial to minimize potential harm to healthy cells. The results of our study suggest that compound **3b** exerts minimal cytotoxicity on MCF-10A cells (IC_{50} = 33.7 ± 2.04 μM) compared to the widely recognized anticancer drug staurosporine (IC_{50} = 26.7 ± 1.62 μM). These results indicate that compound **3b** exhibits a comparable level of selectivity towards cancer cells relative to staurosporine. Collectively, our research

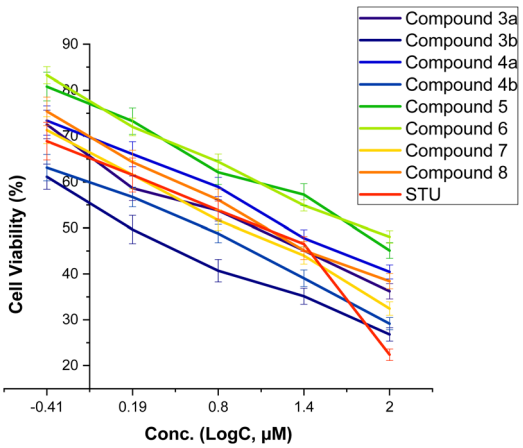

Fig. 3 The dose-dependent effect of compounds (**3–8**) on the cell viability of MCF-7 cells.

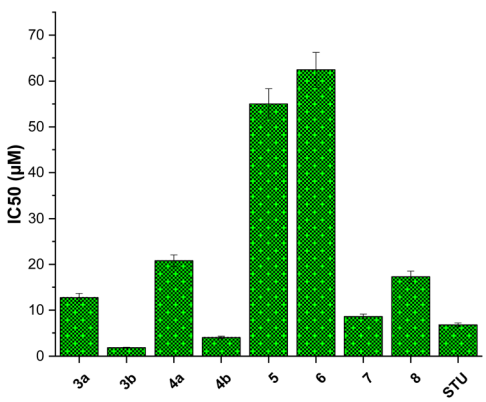

Fig. 4 The inhibitory concentration values (IC_{50}) of synthesized 2-substituted-quinoxaline analogues toward cellular viability of MCF-7 cells.

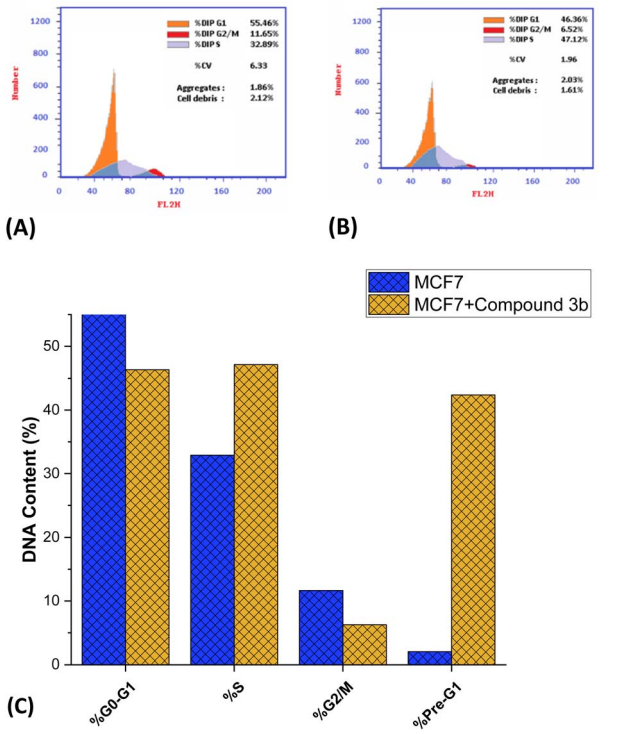

Fig. 5 Impact of compound **3b** (1.85 μM) on the cell cycle of MCF7 cells. Data in histogram format illustrating the distribution of cell cycles in both treated and untreated MCF-7 cells (A and B). (C) Presentation of DNA content percentages in distinct phases of the cell cycle for both untreated and compound **3b**-treated MCF7 cells.

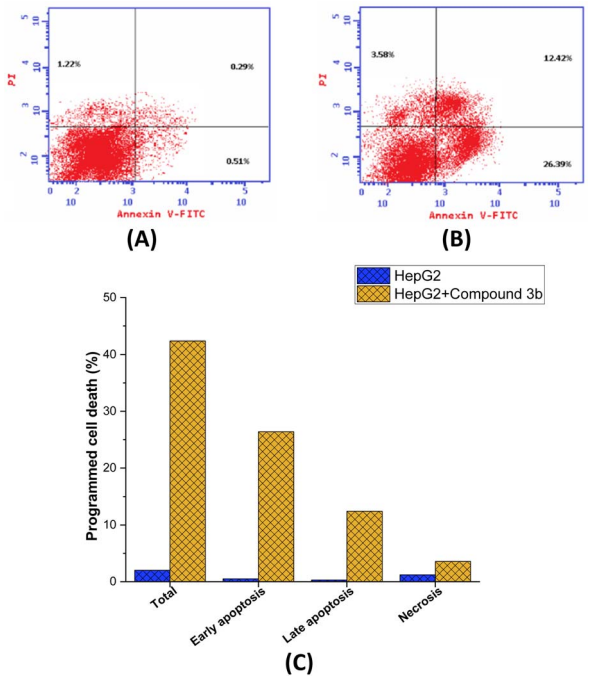

Fig. 6 Induction of programmed cell death in MCF7 cells by compound **3b** treatment. (A) Flow cytometric analysis of MCF7 cells (B) flow cytometric analysis of compound **3b**-treated MCF7 cells (1.85 μM) (C) graphical analysis of the programmed cell death in MCF-7 cells (untreated and treated).

underscores the promise of the presented 2-substituted-quinoxaline analogues promising scaffold for the development of innovative anticancer agents for breast cancer. The potent inhibitory impact of compound **3b** on MCF-7 cells, coupled with its relatively lower toxicity towards normal MCF-10A cells, underscores its promising potential as a foundational structure for the advancement of breast cancer therapeutics (Fig. 5).

Assessment of cell cycle arrest

Encouraged by the anti-proliferative activity of synthesized compounds, our research efforts were directed towards assessing the impact of compound **3b** on the cellular progression through the cell cycle of MCF-7 cells, using flow cytometric techniques. The cells were subjected to compound **3b** at a concentration equivalent to the IC_{50} value. Subsequently, an analysis of the cell cycle distribution was performed, and the obtained findings were compared to those of untreated control cells. As depicted in Fig. 6, our findings demonstrated a significant alteration in the cell cycle distribution following exposure to compound **3b**. Treatment with compound **3b** led to a noticeable shift in the cell population within the G0/G1 and S phases. Specifically, the percentage of cells in the G0/G1 phase decreased from the initial 55.46% to a final 46.36%. In contrast, the proportion of cells in the S phase increased from 32.89% to 47.12% after treatment. On the other hand, a substantial decrease in the cell population was observed at the G2/M phase, while a remarkable increase was seen in the pre-G1 phases. The data indicates a significant reduction in the percentage of cells in the G2/M phase, declining from 11.65% to 6.52%. Conversely, there was a substantial surge in the percentage of cells in the pre-G1 phase, rising dramatically from 2.02% to 42.39%. Our findings suggest that the administration of compound **3b** leads to a substantial decrease in the proportion of cells in the G0/G1 and G1/S phases, implying that it slows down cellular proliferation, especially during these phases. The G0/G1 phase, also known as the first gap phase,[67] is a crucial stage in the cell cycle[68] during which cells undergo a period of rest[69] and preparation for subsequent events such as DNA replication and cell division. It seems that the influence of compound **3b** on the S phase, where DNA replication occurs, is relatively limited. Furthermore, it is worth noting that there has been a significant reduction in the number of cells in the G2/M phase, which indicates that compound **3b** does not induce cell cycle arrest specifically at the G2/M checkpoint. The cell's meticulous oversight of DNA replication's completion and accuracy prior to entering mitosis represents a pivotal control point.[70] However, compound **3b** exhibits a distinct mechanism of action as an anticancer agent. The decline in cellular population within the G2/M phase, as observed, suggests that compound **3b** exhibits inhibitory effects on cell cycle progression beyond this particular stage. This phenomenon may be attributed to the compound's potential influence on proteins associated with G2/M transition or the formation of the mitotic

spindle.[71] The most notable observation entailed a significant increase in the pre-G1 population subsequent to the administration of compound **3b**. The pre-G1 phase, also known as the gap 0 phase, has been observed to be closely linked with the occurrence of apoptosis, a highly regulated and orchestrated process of programmed cell death.[72] The observed substantial augmentation in the population of cells residing in the pre-G1 phase of the cell cycle strongly implies that the administration of compound **3b** exerts a notable influence on the induction of programmed cell death in MCF-7 cells. These findings suggest that compound **3b** induces the initiation of apoptotic signaling cascades, resulting in the fragmentation and degradation of cellular DNA, ultimately culminating in cellular demise. Overall, the presented flow cytometric analysis demonstrates that compound **3b** exhibits a significant impact on cell growth, specifically by inducing cell cycle arrest, through its ability to alter the proportion of cells arrested in the G0-G1, S phase, G1/S and pre-G1 phases.

Assessment of programmed cell death

Subsequently, an investigation was carried out utilizing Annexin V-FITC/PI screening methodology in order to delve deeper into the effects of compound **3b** on the proliferation of MCF-7 cells and to comprehensively assess the occurrence of programmed cell death. The Annexin V-FITC/PI assay is a well-established and commonly employed technique in the field of cell biology.[73] It serves as a valuable tool for distinguishing between apoptotic[74] and necrotic[75] in cells by assessing their respective membrane integrity and phospholipid exposure. As presented in Fig. 6, it is evident that the administration of compound **3b** led to a significant augmentation in the overall proportion of programmed cell death observed in MCF-7 cells. After being exposed to compound **3b**, cells saw a dramatic 21-fold increase in programmed cell death, from 2.02% in untreated cells to 42.39% in treated cell. The results also showed that compound **3b** significantly increased the proportion of apoptosis in MCF-7 cells during both the early and late periods. Treatment with compound **3b** resulted in a 51.7-fold increase in the proportion of cells experiencing early apoptosis, from 0.51% to 26.39% (control untreated to treated cells, respectively). The proportion of cells undergoing late-stage apoptosis also increased dramatically following treatment with compound **3b**, elevating from 0.29% in the control cells to 12.42% in compound **3b**-treated cells. However, compound **3b** did not significantly affect the necrosis pathway in MCF-7 cells. After treatment with compound **3b**, the proportion of cells suffering necrosis considerably increased from 1.2% in untreated cells to 3.58%. The mechanism by which compound **3b** induces cell death in MCF-7 cells has been elucidated to a greater extent through the insights gained from the Annexin V FITC/PI screening. Compound **3b** effectively promoted cell death in MCF-7 cells, as shown by a significant increase in the overall percentage of programmed cell death after treatment. The fact that compound **3b** significantly upregulated early and late apoptosis shows that it activates the apoptotic pathway at various stages, ultimately resulting in cell death. Notably, compound **3b** seems to promote apoptosis rather than necrosis in MCF-7 cells, since necrosis was not significantly affected. Overall, these findings suggest that the observed anti-proliferative activity of compound **3b** in MCF7 cells may be ascribed to its significant induction of the apoptotic pathway within these cells.

Assessment of DNA topoisomerase II activity

The enzyme family topoisomerase II, commonly known as DNA gyrase,[76] plays a crucial role in preserving the three-dimensional structure of DNA.[77] Their capacity to control DNA supercoiling,[78] unlink DNA strands,[79] and resolve DNA tangles[80] is crucial to a number of cellular processes, including replication, transcription, and recombination. Two isoforms of topoisomerase II, topo II and topo II, have been identified.[81] The N-terminal domain of topoisomerase is the DNA-binding region, which finds and binds to target sequences of DNA.[82] The central catalytic domain is the enzyme's active site, where cleavage and re-ligation processes occur.[14] The C-terminal domain contains areas important in dimerization (creating a functioning enzyme complex) and interactions with other proteins,[83] while the N-terminal domain contains a conserved tyrosine residue that forms a covalent intermediate with the DNA during the cleavage process. The presence of this domain adds to the enzyme's interactions with other cellular components and helps stabilize the enzyme's overall structure.[84] Toward this, we aimed to explore whether the anti-proliferative activity of compound **3b** is associated to its ability to target topoisomerase II enzyme in MCF-7 cells. As depicted in Fig. 7, compound **3b** exhibited substantial inhibitory activity against the topo II enzyme, demonstrating a 6.5-fold reduction in comparison to the untreated control cells. This suggests that compound **3b** interferes with the enzyme's ability to alleviate DNA supercoiling or facilitate strand breakage and re-ligation. Consequently, this interference could disrupt DNA replication, transcription, and repair processes, potentially leading to cell cycle arrest and eventual cell death. These findings indicate that the anti-proliferative activity of compound **3b** toward MCF-7 cells could be linked to its ability to target topoisomerase II enzyme.

Molecular docking analysis

Oncology research often aims to discover new molecular predictors for prognosis and treatment response.[85] This shift will transition cancer therapy from non-targeted to targeted

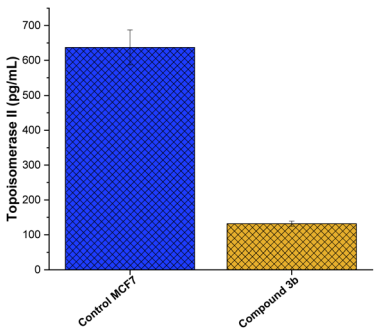

Fig. 7 Inhibitory activity of compound **3b** against topoisomerase II enzyme activity in MCF7 cells.

agents based on patients' tumor molecular characteristics. EGFR, also known as epidermal growth factor receptor, is a type of receptor protein categorized under the family of tyrosine.[86] Tyrosine kinases are enzymes with the essential function of transmitting signals within cells by adding phosphate groups to specific tyrosine residues on target proteins. The activation of EGFR, triggered by binding with ligands, initiates a cascade of cellular reactions, including processes like cell growth, division, and differentiation.[87] This receptor plays a critical role in various biological activities, both normal and pathological, such as cancer. In cancer therapy, a significant approach involves targeting the tyrosine kinase activity of EGFR to disrupt abnormal signaling pathways and hinder the proliferation of tumors. EGFR family members like EGFR, HER2, ErbB3, and ErbB4 are key cancer molecular targets.[86] EGFR overexpression in breast cancer correlates with large tumor size, poor differentiation, and unfavorable outcomes, particularly in aggressive subtypes like triple-negative and inflammatory breast cancer. Considering the background literature,[88] we carried out molecular docking simulations for the current set of compounds using the Glide module from Schrödinger, LLC, NY, 2023. The binding pocket for our synthesized compounds displayed analogous amino acid residues as seen from internal ligand. Fig. 8 depicts the overlay of the optimal docked candidate, **3b**, with a docking score of −11.49 kcal mol^{-1} against the selected target (PDB ID: 1M17). The **3b** (1,2-dihydro isomer) engaged with specific amino acid residues include Leu 694 (π-sigma), Leu 768 (alkyl), Leu 820 (alkyl), Ala 179, Lys 721 (alkyl or π-alkyl interactions), Met 769 and Thr 766 (conventional H-bonding), Pro 770 and Thr 830 (carbon hydrogen bond and Pi-donor H-bond, respectively). Met 742 showed π–sulfur interaction. These interactions encompassed diverse types such as hydrogen bonding, hydrophobic, and positively charged interactions, as detailed in Table 1. Conversely, the **3b** (1,4-dihydro isomer) (docking score: −10.73 kcal mol^{-1}), displayed considerable interactions (Fig. S10†). Additionally, Fig. 9 portrays the binding pocket for the selected standard, staurosporine (STU), which attained a docking score of −9.62 kcal-mol^{-1}. The native co-crystallized ligand, AQ4 exhibited only one H-bonding interaction with Met 769 amino acid. Other residues were Ala 719, Lys 764 and Lys 721 (alkyl typed), Leu 820 and Leu 964 (Pi-Sigma). Nevertheless, we achieved higher affinity of **3b** towards the chosen target than the co-crystallized ligand, AQ4 as depicted in Fig. 8.

Furthermore, the evaluation of the compounds' impact on inhibiting human topoisomerase II (PDB ID: 5GWK) was conducted, with **3b** (1,2 dihydro isomer) consistently emerging as the top docked candidate, achieving a docking score of −13.72 kcal mol^{-1}. The alignment of the best docked **3b** is

Table 1 The interactions formed between best docked **3b** and active site epidermal growth factor receptor tyrosine kinase (PDB ID: 1M17)

Residues	Interaction/residue type	Distance (Å)
Leu 694	π-sigma	3.98
Leu 768, Leu 820	Alkyl	5.12, 4.76
Ala 719, Lys 721	π-alkyl	4.85, 5.19
Pro 770, Thr 830	Hydrogen bond	2.51, 3.44
Met 742	Pi-sulfur	5.53
Met 769	Conventional H-bond	2.98
Thr 766	Conventional H-bond	2.84

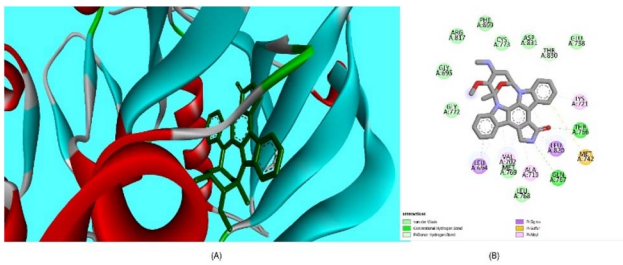

Fig. 9 (A) Compound staurosporine (STU) (green) (standard) superimposed in the active site pocket (PDB ID: 1M17)*(3D); (B) 2D predicted binding mode of the compound **STU** in the active site (H-bond: green, hydrophobic interaction: pink). *This figure was created by using Discovery Studio 4.0 Client (https://discover.3ds.com/discovery-studio-visualizer-download).

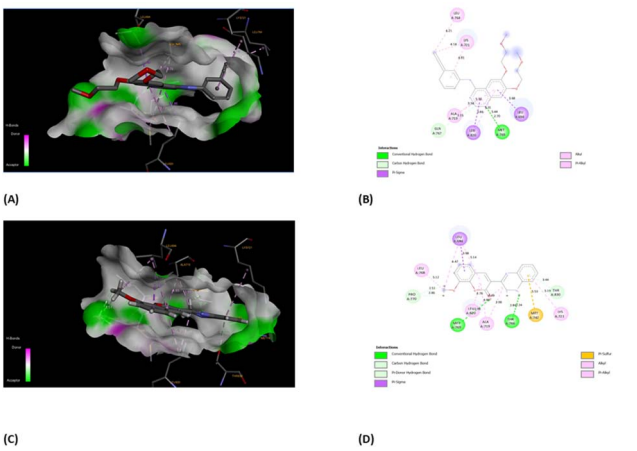

Fig. 8 Descriptive 2D and 3D binding modes* of AQ4, co-crystallized ligand (A and B) and compound **3b** (C and D) inside the pocket of the kinase domain from the epidermal growth factor receptor (EGFRK) (PDB code: 1M17). *This figure was created by using Discovery Studio 4.0 Client (https://discover.3ds.com/discovery-studio-visualizer-download).

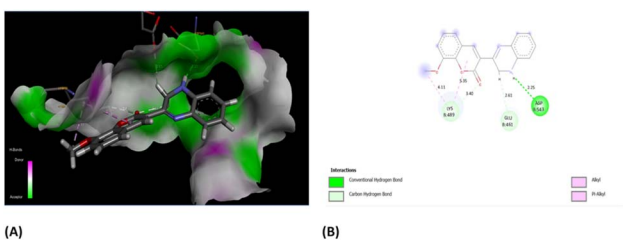

Fig. 10 (A) Compound **3b** (1,2-dihydro isomer) superimposed in the active site pocket (PDB ID: 5GWK)*(3D); (B) 2D predicted binding mode of the compound **3b** in the active site. *This figure was created by using Discovery Studio 4.0 Client (https://discover.3ds.com/discovery-studio-visualizer-download).

Table 2 The interactions formed between best docked **3b** and active site human topoisomerase II (PDB ID: 5GWK)

Residues	Interaction/residue type	Distance (Å)
Glu 461	Carbon hydrogen bond	2.61
Lys 489	Alkyl	4.11, 5.35
Asp 463	Conventional H-bond	2.25

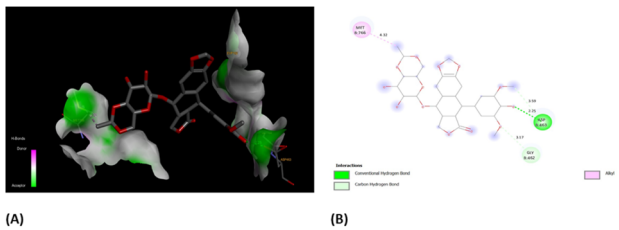

Fig. 11 (A) 3D- and (B) 2D-binding pocket for the co-crystallized ligand, EVP within the target, human topoisomerase II (PDB ID: 5GWK).

depicted in Fig. 10. Remarkably, **3b** maintained a notably higher docking score of −13.72 kcal mol^{-1} in contrast to the standard etoposide's score of −9.61 kcal mol^{-1}. Noteworthy, interactions were observed, including conventional H-bonding interaction with Asp 543 amino acid residue. Amino acid residues Lys 489 and Glu 461 yielded alkyl interactions and carbon hydrogen bond interactions, respectively as detailed in Table 2. Further, the **3b** (1,4-dihydro isomer) exhibited considerable interactions similar to that of 1,2-dihydro isomer (Fig. S11†) Fig. 10.

In order to have better insights from binding scores of native co-crystalized ligands, *i.e.*, (EVP) and obtained best docked molecules, **3b**, we carried out molecular docking of EVP on human topoisomerase II (PDB ID: 5GWK) (Fig. 11(A)). It was found that docking score of EVP was −12.58 kcal mol^{-1}, which was lower than that of **3b**. Furthermore, EVP interacted with similar amino acids as of **3b** such as Asp 463, Gly 462, and Met 766. These findings strongly suggest the potential of compound **3b** as an inhibitor for both EGFR and human topoisomerase II, underscoring the need for further exploration through *in vivo* experiments.

Molecular dynamics (MD) analysis

The molecular dynamics simulations (MD) were employed to evaluate the stability of the top docked ligand, 1M17_3b, in relation to the target. This analysis was conducted over a 150 ns simulation duration using the software 'Desmond' by Schrödinger, LLC, New York, 2023. The comprehensive MD system comprised 34 246 atoms, including 9896 water molecules, as illustrated in Fig. 12(a)–(f). In these simulations, we gauged the average displacements of atoms relative to a specific timeframe using the 'RMSD' (Root Mean Square Deviation) parameter. Our examination of the RMSD parameter disclosed a consistently stable conformation. When the ligand **3b** (1,2-dihydro isomer) was bound to the target 1M17, the Cα-RMSD backbone RMSD values were consistently under 3.5 Å, and 'Lig_fit_Prot' values

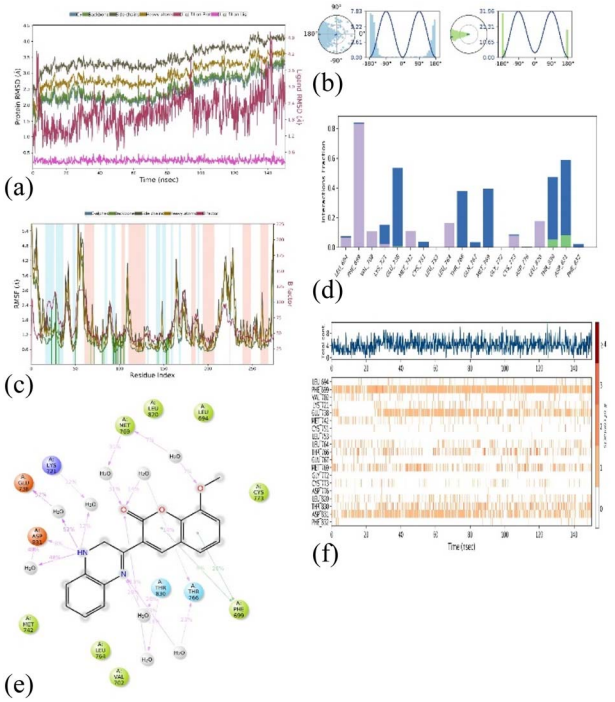

Fig. 12 MD simulation analysis for complex 1M17_3b (1,2-dihydro isomer) (a) RMSD plot; (b) RMSF analysis; (c) ligand–protein contact plot; (d) ligand torsion profile; (e) protein–ligand interaction plot; and (f) a timeline representation plot representing such interactions with amino acid residues over the simulation period of 150 ns.

were maintained below 0.5 Å, as depicted in Fig. 12a. Throughout the 0–150 ns period, the entire complex exhibited enduring stability. Moreover, localized fluctuations within the protein chains were scrutinized through the 'RMSF' (Root Mean Square Fluctuation) plot, detailed in Fig. 12b. While there were minor spikes in fluctuation for specific amino acids, these variations didn't lead to significant changes, indicating their inherent flexibility. The analysis of the 'protein–ligand' interaction plot (Fig. 12c) revealed crucial interactions, including hydrophobic interactions with amino acids Leu 694, Phe 699, Lys 721, Met 742, Leu 764, Cys 773, and Leu 820. No ionic interactions were observed, but there were hydrogen bonds with Thr 830 and Asp 831, along with water bridges involving residues like Lys 721, Leu 694, Glu 738, Cys 751, Thr 766, Gln 767, Met 769, Thr 830, and Phe 832. Fig. 12f presented a timeline representation of these interactions with amino acid residues throughout the 150 ns simulation period. In Fig. 12e, the 'ligand–protein' contact plot highlighted interactions occurring more than 5.0% of the simulation time (Met 769: 31%, Lys 721: 12%, Glu 738: 52%, Asp 831: 8%, Thr 830: 28%, Thr 766: 23%, and Phe 699: 28%) within the chosen trajectory (0.00–150.00 ns). The 'ligand torsions plot' (Fig. 12d) summarized the conformational changes of each rotatable bond (RB) in the ligand during the simulation trajectory (0.00–150.00 ns). These results indicate that the ligand–protein conformation remained stable throughout the 150 ns simulation period. Additionally, we extended our analysis to explore the stability of the 1M17_3b

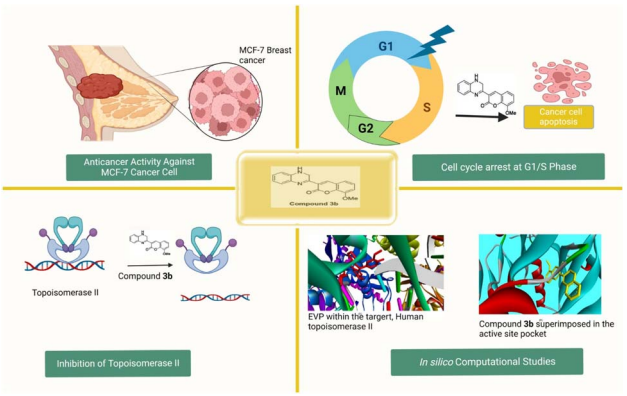

Fig. 13 Summary of the anti-proliferative activity of compound **3b** toward MCF7 cells.

(1,4-dihydro isomer), in relation to the target. This analysis was conducted over a 150 ns simulation duration. The comprehensive MD system comprised 34 246 atoms, including 9896 water molecules, as illustrated in Fig. S12(a)–(f).†

Taken together, these findings present compelling evidence for the therapeutic potential of the newly developed class of quinoxaline analogs. These analogs, including compound **3b**, exhibited considerable anti-cancer properties against MCF-7 cells, surpassing established drugs like staurosporine with lower toxicity to normal cells. Compound **3b** demonstrated its ability to significantly arrest the cell cycle, induce apoptosis, and inhibit topoisomerase II activity, disrupting critical processes in cancer cells. Molecular modeling and molecular simulation assessments showed its affinity for EGFR, strengthening its potential as a breast cancer treatment (Fig. 13). While promising, further research, including *in vivo* trials, is needed. Nonetheless, this study lays the groundwork for a novel and effective class of breast cancer treatments, offering insights into their mechanisms of action for future drug development.

Experimental

Instruments and analytical techniques

The acquisition of the ^{1}H-NMR and ^{13}C-NMR spectra was performed utilizing a Bruker Avance Av-400 instrument. The chemical shifts observed in the spectra were meticulously recorded in parts per million (ppm) relative to the standard compound tetramethyl silane (TMS), a common reference point in the field of nuclear magnetic resonance (NMR) spectroscopy. The IR data was acquired utilizing the Shimadzu 470 spectrometer. The compounds underwent analysis utilizing an electron ionization (ET) mass spectrometer, specifically employing a probe Agilent MSD 5975 spectrometer. The instrument was configured to operate at an energy level of 70 electron volts (eV). The determination of the melting point was conducted utilizing an electrothermal 200 digital melting point apparatus, with the obtained results not being adjusted for potential temperature fluctuations. The elemental analysis was conducted utilizing an Aferkinelmer 2400 series CHN elemental analyzer. With the exception of any explicitly stated conditions, all chemicals were procured from a commercial supplier and utilized without undergoing subsequent purification procedures.[89]

Synthetic procedure

General procedure for the syntheses of 2-substituted dihydro quinoxaline (3a & 3b). A solution of compound **2a** or **2b** (0.01 mol, prepared as previously reported[65,66]), phenylene-1,2-diamine (0.01 mole), and fused sodium acetate (0.03 mol) in 50 mL of absolute ethanol was subjected to reflux for a duration of 12 h. The reaction mixture underwent a cooling process, followed by careful pouring into water while simultaneously stirring. Consequently, the resulting solid was isolated through the application of filtration. The solid was then subjected to a thorough washing with hot water, subsequent drying, and ultimately recrystallization from a suitable solvent. This meticulous procedure successfully yielded compound **3(a, b)**.

*2-(5-Bromo-2-hydroxyphenyl)-3,4-dihydroquinoxaline (**3a**).* A orange crystals, yield 56%, m.p. 210 °C. IR (kBr) $\gamma_{max} = 3461$ (br-OH), 3221 (NH), 1625 (C=N), 1605, 1588 (C=C), 1046 (C=O) cm^{-1}. ^{1}H-NMR (DMSO-d$_6$, ppm, 400 MHz) δ: 4.40 (t, 2H, NCH$_2$), 7.02–8.41 (m, 9H, Ar–H, NH, and H-3 of quinoxaline of two isomers), 9.68, 9.72 (s, 2H, 2*NH of 1,4-dihydroquinoxaline), 12.18, 12.45 (s, 1H, OH of two isomers). ^{13}C-NMR (DMSO-d$_6$, ppm, 100 MHz) δ: 159.04, 157.61, 152.26, 150.55, 145.82, 145.42, 141.04, 140.80, 140.19, 139.63, 136.77, 135.07, 140.19, 139.63, 136.77, 135.07, 133.49, 132.06, 131.92, 131.41, 131.37, 130.74, 130.42, 129.63, 129.33, 128.95, 128.59, 123.02, 120.08, 119.97, 118.02, 111.26, 56.50. MS analysis (*m*/*z*, %): 302 (100), 299 (43.17), 274 (6.68), 221 (31.52), 193 (29.27), 166 (5.73), 118 (2.87), 111 (2.80), 102 (4.56), 96 (4.02), 77 (6.35), 63 (2.98). Anal. calcd. for C$_{14}$H$_{11}$BrN$_2$O (M_{wt} = 302): C, 55.63; H, 3.64; N, 9.27. Found: C, 55.48; H, 3.46; N, 9.09.

*2-(8-Methoxy-coumarin-3yl)-3,4-dihydroquinoxaline (**3b**).* A yellow crystals, yield 61%, m.p. 235 °C. IR (kBr) γ_{max} = 3225 (NH), 1729 (C=O), 1631 (C=N), 1605, 1589 (C=C), 1172, 1083 (C–O) cm^{-1}. ^{1}H NMR (DMSO-d$_6$, ppm, 400 MHz) δ: 3.95, 3.97 (s, 3H, OCH$_3$ of two isomers), 4.02 (s, 2H, NCH$_2$ of quinoxaline ring), 6.43–8.19 (m, 9H, Ar–H, H-3 of quinoxaline and NH), 8.89 (s, 1H, H-4 of coumarin ring), 9.60 (s, 1H, NH), 11.41 (s, 1H, NH). ^{13}C-NMR (DMSO-d$_6$, ppm, 100 MHz) δ: 159.84 (C=O of coumarin ring), 148.22, 147.75, 147.31, 146.83, 146.70, 145.83, 145.27, 143.60, 141.89, 141.72, 141.13, 131.26, 131.15, 129.57, 129.35, 125.42, 125.32, 125.15, 124.16, 123.84, 122.12, 121.26, 120.10, 119.15, 118.89, 116.87, 115.82, 114.32, 112.59 (carbons of quinoxaline and coumarin rings of two isomers), 56.67, 56.57 (OCH$_3$ of two isomers), 30.51 (NHCH$_2$). MS analysis (*m*/*z*, %); 306 (16.30), 304 (100), 276 (16.95), 261 (7.32), 219 (9.08), 205 (12.88), 177 (10.56), 159 (3.55), 152 (8.82), 119 (3.83), 109 (3.04), 102 (17.32), 76 (8.40). Anal. calcd. for C$_{18}$H$_{14}$N$_2$O$_3$ (M_{wt} = 306): C, 70.59; H, 4.57; N, 9.15. Found: C, 70.33; H, 4.27; N, 9.01.

General procedure for the syntheses of 2-(substituted)-quinoxaline (4a, 4b). A solution of compound **3(a, b)** (0.01 mole) was subjected to reflux in the presence of 20 mL of acetic anhydride for a duration of 14 h. Following this, the resulting

mixture was allowed to cool and subsequently added to ice-water while being vigorously stirred. After allowing the reaction mixture to stand for a duration of 24 h, the resulting product was separated from the mixture through the process of filtration. The isolated product was then subjected to a thorough washing with water, followed by a drying process. Subsequently, the product was subjected to recrystallization, utilizing an appropriate solvent, resulting in the formation of compounds **4a** and **4b**.

*2-(2-Acetoxy-5-bromo) phenyl quinoxaline (**4a**).* A pale orang crystal, yield 73%, m.p. 187 °C. IR (kBr) γ_{max} = 1763 (C=O), 1632 (C=N), 1608, 1584 (C=C), 1113, 1066 (C–O) cm^{-1}. ^{1}H-NMR (DMSO-d_6, ppm, 400 MHz) δ: 2.22 (s, 3H, $COCH_3$), 7.37–7.39 (d, 1H, ArH), 7.83–7.96 (m, 3H, Ar–H), 8.15–8.19 (m, 3H, Ar–H), 9.26 (s, 1H, CH=N of quinoxaline). ^{13}C-NMR (DMSO-d_6, ppm, 100 MHz) δ: 169.48 (C=O), 149.51, 148.16, 145.74, 141.72, 141.28, 134.12, 133.84, 132.30, 131.40, 131.26, 129.74, 129.39, 126.71, 119.31 (C-aromatic and quinoxaline ring), 21.19 (CH_3). MS analysis (*m*/*z*, %); 342 (2.50), 315 (3, 50), 302 (83.21), 300 (100), 272 (5.28), 221 (14,69), 193 (20.32), 164 (6.69), 102 (6.77). Anal. calcd. for $C_{16}H_{11}BrN_2O_2$ (M_{wt} = 342): C, 56.14; H, 3.21; N, 8.19. Found: C, 55.89; H, 3.01; N, 8.03.

*2-(8-Methoxycoumarin-3-yl)-quinoxaline (**4b**).* As pale-yellow crystal, yield 69%, m.p. 168 °C. IR (kBr) γ_{max} = 1731 (C=O), 1633 (C=N), 1609, 1592 (C=C), 1213, 1073(C–O) cm^{-1}. ^{1}H-NMR (DMSO-d_6, ppm, 400 MHz) δ: 3.92, 3.97 (s, 3H, OCH_3 of two isomers), 6.56–6.18 (m, 7H, ArH), 8.89 (s, 1H, H-4 of coumarin), 9.60 (s, 1H, CH=N of quinoxaline). ^{13}C NMR (DMSO-d_6, ppm, 100 MHz) δ: 159.84 (C=O), 148.75, 148.23, 146.82, 145.83, 145.27, 143.60, 141.88, 141.72, 131.25, 131.15, 129.56, 129.35, 125.42, 124.17, 121.26, 120.11, 119.18, 118.02, 115.81, 114.34 (carbons of coumarin and quinoxaline rings), 56.67, 56.16, 21.19 (OCH_3 of two stereo isomers). MS analysis (*m*/*z*, %); 304 (100), 276 (6.68), 240 (20.35), 205 (8.71), 191 (11.00), 153 (6.29), 144 (4.44), 132 (5.30), 102 (18.82), 76 (21.46), 50 (8.34). Anal. calcd. for $C_{18}H_{12}N_2O_3$ (M_{wt} = 304): C, 71.5; H, 3.95; N, 9.21. Found: C, 70.91; H, 3.66; N, 9.03.

*Synthesis of 2-(5-bromo-8-methoxy-coumarin-3-yl)-quinoxaline (**5**).* Compound **4b** (0.01 mole) was dissolved in 20 mL of glacial acetic acid at ambient temperature. Subsequently, a solution containing 10 mL of bromine (equivalent to 0.01 moles) dissolved in glacial acetic acid was meticulously introduced in a dropwise manner to compound **4b**, while maintaining a constant stirring rate within the temperature range of 40–60 °C. Following a time interval of 5–10 minutes, the characteristic hue of bromine was observed to dissipate, leaving behind a solution of a yellow nature. Subsequently, a volume of 1 mL of bromine solution was meticulously introduced into the experimental setup, while ensuring continuous agitation, and maintained at ambient temperature for a duration of 8 h. The resultant reaction mixture was carefully introduced into a ice-water, while being subjected to continuous agitation. Subsequently, the resultant solid precipitate was carefully collected through the process of filtration, followed by thorough rinsing with water and subsequent desiccation to achieve complete dryness. After a series of experimental procedures, the product underwent a crystallization process utilizing ethanol as the solvent, resulting in the formation of compound **5** in the form of vibrant orange crystals. The overall yield of this crystallization process was determined to be 82%. The melting point of compound **5** was 205 °C. IR (kBr) γ_{max} = 1735 (C=O), 1632 (C=N), 1608, 1587 (C=C), 1121, 1064 (C–O) cm^{-1}. ^{1}H-NMR (DMSO-d_6, ppm, 400 MHz) δ: 3.96, 4.12 (s, 3H, OCH_3 of two isotopes of compound **5**), 6.56–8.23 (m, 6H, ArH), 8.77, 8.87 (s, 1H, H-4 of coumarin), 9.61, 9.64 (s, 1H, CH=N of quinoxaline of two isomers). ^{13}C-NMR (DMSO-d_6, ppm, 100 MHz) δ: 164.48 (C=O), 163.30, 163.16, 155.18, 149.58, 147.37, 146.16, 145.90, 143.80, 141.90, 131.40, 129.35, 128.79, 116.35, 115.79 (carbons of coumarin and quinoxaline rings), 56.97, 56.70 (OCH_3 of the two isomers). MS analysis (*m*/*z*, %); 384 (79.35), 383 (22.62), 382 (100), 354 (10.33), 311 (14.81), 303 (35.53), 285 (12.42), 275 (68.95), 247 (22.64), 232 (17.21), 219 (16.10), 204 (37.93), 191 (14.07), 177 (33.79), 153 (17.36), 144 (9.75), 129 (19.84), 116 (4.19), 102 (41.41), 96 (29.29), 82 (100), 80 (95.78), 79 (44.58), 76 (31.54). Anal. calcd. for $C_{18}H_{11}BrN_2O_3$ (M_{wt} = 382): C, 56.54; H, 2.88; N, 7.33. Found: C, 56.25; H, 2.59; N, 7.11.

*Synthesis of ethyl [3-(5-bromo-2-hydroxy phenyl)-1,4-dihydroquinoxalin-1-yl] acetate (**6**).* A solution of compound **3a** (0.01 mole) and ethyl chloroacetate (0.01 mole) in dimethyl formamide (25 mL) was subjected to reflux for a duration of 12 hours in the presence of triethylamine (2 mL). The reaction mixture underwent a cooling process, followed by its transfer into a solution of ice-water. Subsequently, the mixture was subjected to neutralization using diluted aqueous hydrochloric acid (2%) under continuous stirring. The solid obtained from the experimental procedure was effectively isolated through the process of filtration and subsequently subjected to recrystallization using ethanol as the solvent. This recrystallization step yielded pale-yellow crystals (68%). The melting point of compound **6** was found to be 169 °C. IR (kBr) γ_{max} = 3465 (br.OH), 3212 (NH), 1763 (C=O), 1605, 1587 (C=C), 1121, 1093 (C–O) cm^{-1}. ^{1}H NMR (DMSO-d_6, ppm, 400 MHz) δ: 1.22 (t, 3H, CH_3), 4.20 (q, 2H, OCH_2), 5.02 (s, 2H, NCH_2CO), 7.03–8.31 (m, 8H, Ar–H and H-3 of quinoxaline of two stereo isomers), 9.53, 9.69 (s, 1H, NH of two isomers), 12.19 (s, 1H, OH). ^{13}C-NMR (DMSO-d_6, ppm, 100 MHz) δ: 168.79 (C=O), 159.06, 157.63, 155.30, 150.84, 150.32, 147.30, 145.80, 142.23, 141.14, 141.05, 140.17, 135.06, 134.35, 133.87, 132.04, 131.36, 130.91, 130.78, 129.74, 129.30, 129.25, 128.04, 123.00, 120.09, 115.98, 113.84, 111.26 (carbons of aromatic and quinoxaline rings), 65.83 (NCH_2CO), 61.38 (OCH_2), 14.47 (CH_3). Anal. calcd. for $C_{18}H_{17}BrN_2O_3$ (M_{wt} = 388): C, 55.67; H, 4.38; N, 7.22. Found: C, 55.44; H, 4.11; N, 7.02.

Synthesis of 2-(5-bromo-3-phenylazo-2-hydroxyphenyl)-1,4-dihydro quinoxaline (7). A solution of compound **3a** (0.01 mole) was prepared by dissolving it in 10 mL of aqueous sodium hydroxide (10%). The resulting solution was then cooled using an ice bath to a temperature range of 0–5 °C. An aqueous solution (at −5 °C) containing the phenyl diazonium salt (0.01 mole) was meticulously introduced in a gradual manner with continuous agitation over a period of 15 minutes. Following the addition, the resulting reaction mixture was subjected to stirring for an additional duration of 30 minutes, after which it was subsequently allowed to stand at −5 °C for a period of 24 h. The

resultant precipitate was meticulously collected through the process of filtration, followed by thorough washing with water. Subsequently, it was subjected to a meticulous drying procedure. In order to achieve optimal purity, the compound was further purified through a detailed crystallization process utilizing ethanol as the solvent. The purification process yielded compound **7** in the form of striking red crystals, with a yield of 71%. The compound exhibited a melting point of 242 °C. IR (kBr) γ_{max} = 3467 (OH), 3227 (NH), 1605, 1588 (C=C), 1121, 1081 (C–O) cm^{-1}. ^1H NMR (DMSO-d_6, ppm, 400 MHz) δ: 4.52 (s, 2H, NCH_2), 6.47–8.30 (m, 12H, Ar–H and H-3 Of quinoxaline of two isomers), 9.68 (s, 1H, NH), 12.10 (S, 1H, OH), 14.88 (S, 1H, OH) PPM. ^{13}C NMR (DMSO-d_6, ppm, 100 MHz) δ: 157.63, 152.30, 151.21, 150.84, 145.80, 145.43, 141.05, 140.17, 135.05, 132.04, 131.35, 130.71, 129.90, 129.30, 128.93, 128.26, 122.99, 122.80, 120.09, 118.03, 114.35, 111.26 (carbon of aromatic and quinoxaline rings), 40.12 (NCH_2). MS analysis (*m*/*z*, %); 406 (1.27), 404 (7.69), 377 (21.35), 326 (31.58), 313 (31.36), 300 (73.69), 271 (42.51), 237 (32.60), 221 (100), 193 (50.04), 178 (13.50), 169 (24.47), 152 (14.14), 139 (11.91), 102 (9.61), 93 (35.00), 77 (33.61). Anal. calcd. for $C_{20}H_{15}BrN_4O$ (M_{wt} = 406): C, 59.11; H, 3.69; N, 13.79. Found: C, 58.98; H, 3.33; N, 13.54.

*Synthesis of 2-(2-acetoxy-3-phenylazo-5-bromo) phenyl quinoxaline (**8**).* Compound **7** (0.01 mole) was dissolved in 25 mL of acetic anhydride. The resulting solution was subjected to reflux for a duration of 16 h, followed by a cooling process. The reaction mixture was carefully transferred into an ice-water bath under continuous agitation and allowed to incubate for a duration of 24 h at 0 °C. The resultant solid crude was separated from the solution through filtration, subsequently subjected to water rinsing, and then dried. To further refine its purity, the crude solid was further purified by re-crystallization technique using ethanol as a solvent. This process yielded compound **8** in the form of pale orange crystals, with a yield of 86%. The melting point assessed as 187 °C. IR (kBr) γ_{max} = 1756 (C=O), 1638 (C=N), 1610, 1588 (C=C), 1131, 1063 (C–O) cm^{-1}. ^1H-NMR (DMSO-d_6, ppm, 400 MHz) δ: 1.74, 2.21 (s, 3H, $COCH_3$ of two isomers), 7.01–8.17 (m, 11H, Ar–H), 9.24 (s, 1H, CH=N of quinoxaline), 9.77 (s, 1H, CH=N of another isomer). ^{13}C-NMR (DMSO-d_6, ppm, 100 MHz) δ: 174.81, 169.41 (C=O), 162.86, 159.81, 151.69, 149,49, 148.14, 146.70, 145.68, 141.72, 141.34, 141.26, 140.87, 134.51, 134.32, 133.80, 132.26, 131.42, 131.26, 130.84, 130.12, 129.72, 129.53, 129.37, 129.19, 128.51, 126.70, 124.33, 121.76, 120.85, 119.31 (carbon of aromatic and quinoxaline rings of two stereo isomers), 24.25, 21.16 (CH_3 of two stereo isomers). MS analysis (*m*/*z*, %); 446 (M^+, unstable), 404 (7.69%), 377 (15.60), 327 (17.78), 300 (49.93), 268 (10.03), 221 (100), 193 (40.95), 77 (14.18). Anal. calcd. for $C_{22}H_{15}BrN_4O_2$ (M_{wt} = 446); C, 59.19; H, 3.36; N, 12.56. Found: C, 58.98; H, 3.11; N, 12.22.

Assessment of anti-proliferative activity

The *in vitro* measurement of cytotoxic activity was conducted for the quinoxaline derivatives utilizing the MTT assay. The cells were seeded into a 96-well multiwall plate at a density of 105 cells per well and allowed to adhere for a period of 24 hours prior to the commencement of compound treatment. The test compounds underwent dissolution in dimethyl sulfoxide (DMSO). Various concentrations of the compound under investigation were introduced to the monolayer of cells. For each specific concentration, a total of three wells were meticulously prepared. The monolayer cells underwent incubation with the compound(s) for a duration of 48 hours at a temperature of 37 °C, within an atmosphere containing 5% carbon dioxide. Following a 48 hour incubation period, cellular specimens were subjected to fixation, thorough washing, and subsequent staining with a 40 μL volume of MTT solution (comprising 5 mg mL^{-1} of MTT in a 0.9% NaCl medium) per well. This staining process was carried out for an additional 4 hour duration under controlled incubation conditions. The MTT crystals were effectively dissolved through the addition of 180 μL of acidified isopropanol per well. The plate was then subjected to gentle agitation at ambient temperature, allowing for optimal solubilization. Subsequently, the absorbance at 570 nm was measured using an ELISA reader, enabling accurate quantification. The determination of the molar concentration necessary to achieve a 50% reduction in cell viability, commonly referred to as the IC_{50} value, was computed and subsequently juxtaposed with the reference pharmaceutical agent, staurosporine.[90–92] The experimental procedures were conducted in triplicate to ensure robustness and reliability of the results.

Assessment of cell cycle arrest

MCF-7 cells were seeded at a density of 3.0×10^5 cells per well and subsequently subjected to incubation at a temperature of 37 °C for a duration of 12 h. After cellular acquisition, the designated cellular entities were subjected to the administration of compound **3b** at a concentration dose value equivalent to its IC_{50}, followed by an incubation period of 48 h. Following the completion of the treatment, cellular specimens were gathered and subjected to fixation using a 75% ethanol solution at a temperature of 20 °C for the duration of 18 h. Subsequently, the cells underwent a thorough rinsing procedure utilizing PBS, followed by centrifugation. The cells were then exposed to a solution containing Rnase (Sigma, USA) at a concentration of 10 mg mL^{-1}, along with propidium iodide (PI, Sigma) at a concentration of 5 mg mL^{-1}. This preparation preceded the subsequent analysis of the cells using flow cytometry, specifically employing the FACS Calibur cytometer in conjunction with Cellquest software, both provided by BD Bioscience, USA.[93,94]

Assessment of apoptosis and necrosis by Annexin-V assay

The MCF-7 cells were subjected to treatment with compound **3b** at a concentration equivalent to its IC_{50} value for a duration of 48 h. Following the therapeutic intervention, cellular entities were procured and subjected to a dual washing procedure involving two cycles of centrifugation (180 g, 10 minutes, 4 °C) using phosphate-buffered saline (PBS). The suspension of each individual cell well was performed by resuspending it in 100 μL of binding buffer, followed by the addition of 5 μL of Annexin V-FITC. Following an incubation period of 10 minutes at ambient

temperature, an additional 400 μL of binding buffer was introduced, resulting in a final volume of 500 μL. The cellular specimens were subjected to staining with propidium iodide (PI) in a prompt manner, just prior to the commencement of the measurement process. The cells were subjected to analysis utilizing the FACS Calibur flow cytometer, a cutting-edge instrument manufactured by Becton and Dickinson in Heidelberg, Germany. The acquired data were subjected to analysis using the Cell-Quest software, developed by Becton and Dickinson in Heidelberg, Germany.

In vitro assessment of topoisomerase II activity

Compound **3b** was chosen as the subject of evaluation in relation to topo II [MBS#942146], employing the utilization of human DNA topoisomerase II-β (TOPII-β) ELISA kit, in accordance with the guidelines provided by the manufacturer. All necessary reagents, working standards, and samples were appropriately prepared in accordance with established protocols and procedures. A total volume of 100 millilitres (mL) of both the standard and sample solutions were introduced into each well, followed by an incubation period of 2 h at a temperature of 37 °C. The aqueous solution was extracted from each well. Subsequently, a volume of 120 μL of biotin-antibody solution was introduced into each well, followed by an incubation period of 1 h at a temperature of 37 °C. The media was extracted utilizing an aspirator and subsequently subjected to a triple washing procedure employing a washing buffer. A volume of 100 pL of Horseradish Peroxidase (HRP-Avidin) was introduced into every well, followed by an incubation period of 1 h at a temperature of 37 °C. The repetition of the aspiration/wash process was performed a total of five cycles. A volume of 90 μL of 3,3′,5,5′-tetramethylbenzidine (TMB) substrate was introduced into every well and subjected to an incubation period of 15–30 minutes at a temperature of 37 °C, ensuring protection from any light exposure. A volume of 50 μL of stop solution was introduced into every well, followed by the prompt measurement of the optical density of each well within a time frame of 5 minutes. This was accomplished using a ROBONEK P2000 enzyme-linked immunosorbent assay (ELISA) reader at a wavelength of 450 nm. The experimental procedures were conducted in triplicate to ensure robustness and reliability of the results.

Molecular docking simulations

For molecular docking simulations, we downloaded a 3D-crystal structure of receptor EGFR tyrosine kinase (Epidermal Growth Factor Receptor tyrosine kinase) (PDB ID: 1M17; resolution: 2.60 Å) from the RCSB website.[88,95] Similarly, a 3D-crystal structure of receptor human topoisomerase II was also downloaded from RCSB databank (PDB ID: 5GWK; resolution: 3.15 Å).[45] We then carried out molecular docking simulations using the popular software module, Glide, Schrodinger, LLC, NY, 2023. The 3D structures of synthesized analogues (ligands) were drawn using the software 'MarvinSketch®' 5.8.3 (2012) and 'ChemAxon' tools. These structures were then imported into Schrödinger's Maestro workflow, and ligand preparation was conducted using the 'LigPrep' module from Schrödinger, LLC, New York (2023). During the docking process, the grid dimensions were maintained as documented in previous research. The docking calculations were performed using the 'XP mode' (Extra precision), with all default parameters. The most favorable docking positions were visualized using Discovery Studio 4.5 (Studio, 2008).[96–101]

Molecular dynamics simulation (MDS) study

For the Molecular Dynamics Simulation (MDS) analysis, we conducted simulations on the complex labelled as '1M17_3b' using the 'Desmond' module developed by Schrödinger, Inc., New York, USA (2023). In this simulation setup, we employed an explicit solvent model, which included TIP3P water molecules and the OPLS-2005 force field. The simulation was performed within a periodic boundary box with dimensions of 10 Å × 10 Å × 10 Å. To maintain a charge balance of 0.15 M, sodium ions (Na^+) were introduced into the system. Additionally, NaCl solutions were incorporated to replicate physiological conditions. The simulation was carried out for a duration of 150 nanoseconds (ns). The specific details of the MD protocol were taken from a previous study conducted by Mishra *et al.*, 2019.[88]

Conclusions

The prevalence of breast cancer among women worldwide presents a significant global public health concern. This paper provided compelling evidence regarding the potential therapeutic effectiveness of a newly developed group of 2-substituted-quinoxaline analogs as potential anticancer agents toward breast cancer. These synthesized quinoxaline derivatives, incorporating phenyl and coumarin components, demonstrate notable antiproliferative properties against MCF-7 cells. Remarkably, compound **3b** exhibited substantial inhibitory potential, with an IC_{50} value of 1.85 ± 0.11 μM, surpassing the inhibitory effects of the established anticancer drug staurosporine, while maintaining low toxicity towards normal cells. Furthermore, our study delved into the mechanisms responsible for the antiproliferative action of compound **3b**, revealing its ability to induce cell cycle arrest at the G1/S phase and initiate apoptosis in MCF-7 cells, with minimal necrosis. Additionally, compound **3b** significantly inhibited topoisomerase II activity, a crucial enzyme involved in DNA replication and repair, suggesting its capacity to disrupt essential biological processes linked to cancer cell development and survival. Moreover, molecular modeling and molecular simulation investigations affirmed the strong affinity of compound **3b** for the active cavity of EGFR, a member of the tyrosine kinase receptor protein family, further supporting its potential as a promising therapeutic agent for breast cancer treatment. The data presented in this study underscores the therapeutic potential of the developed quinoxaline derivatives, particularly those incorporating phenyl and coumarin components, with a specific focus on compound **3b**, in the context of breast cancer treatment. Although these findings are promising, further investigations, including *in vivo* trials, are imperative to validate the efficacy of compound **3b**. Nevertheless, our study

establishes a foundational framework for identifying a novel and highly effective class of compounds against breast cancer, while also shedding light on the underlying mechanisms of their action. These insights provide valuable guidance for future drug development endeavors.

Author contributions

Conceptualization, M. G. S., S. A. A. E., S. N. M., R. A. A., E. M. S., and M. F. Y.; methodology, M. G. S., E. H. E, S. A. A. E., S. N. M., G. A., R. A. A., H. A. A., E. M. S., and M. F. Y.; software, S. N. M., E. H. E, H. A. A., H. A. A., N. A., E. A., E. M. S., and M. F. Y.; validation, S. N. M., H. A. A., G. A., R. A. A., N. A., E. A., M. F. Y.; formal analysis, M. G. S., E. H. E, S. A. A. E., S. N. M., H. A. A., N. A., E. A., and M. F. Y.; investigation, M. G. S., H. A. A., G. A., R. A. A., H. A. A., N. A., E. A., E. M. S., and M. F. Y.; resources, M. G. S., S. A. A. E., E. H. E, S. N. M., H. A. A., R. A. A., N. A., E. A., and M. F. Y.; data curation, M. G. S., S. A. A. E., E. H. E, S. N. M., G. A., R. A. A., E. M. S., and M. F. Y.; writing – original draft preparation, M. G. S., S. A. A. E., S. N. M., E. M. S., and M. F. Y.; writing – review and editing, M. G. S., S. A. A. E., E. H. E, S. N. M., H. A. A., G. A., R. A. A., H. A. A., N. A., E. A., E. M. S., and M. F. Y.; visualization, E. H. E, H. A. A., G. A., R. A. A., H. A. A., N. A., E. A., and M. F. Y.; supervision, M. G. S., S. N. M., E. M. S., and M. F. Y.; project administration, M. G. S., S. A. A. E., S. N. M., R. A. A., E. M. S., and M. F. Y.; funding acquisition, G. A., R. A. A., N. A., E. A., and E. M. S. All authors have read and agreed to the published version of the manuscript.

Conflicts of interest

There are no conflicts to declare.

Acknowledgements

The authors acknowledge the Princess Nourah Bint Abdulrahman University for funding this work through the Researchers Supporting Project number (PNURSP2023R89), Princess Nourah Bint Abdulrahman University, Riyadh, Saudi Arabia. This study was also supported by Researchers Supporting Project number (RSP2023R111), King Saud University, and Riyadh, Saudi Arabia.

Notes and references

1 G. N. Sharma, R. Dave, J. Sanadya, P. Sharma and K. K. Sharma, *J. Adv. Pharm. Technol. Res.*, 2010, **1**, 109–126.
2 R. Snijders, L. Brom, M. Theunissen and M. Van Den Beuken-van Everdingen, *Cancers*, 2023, **15**, 591.
3 F. Cardoso, S. Kyriakides, S. Ohno, F. Penault-Llorca, P. Poortmans, I. T. Rubio, S. Zackrisson and E. Senkus, *Ann. Oncol.*, 2019, **30**, 1194–1220.
4 K. P. McGuire, in *Breast Disease*, ed. A. Aydiner, A. İğci and A. Soran, Springer International Publishing, Cham, 2016, pp. 1–14.
5 M. E. Jones, M. J. Schoemaker, L. B. Wright, A. Ashworth and A. J. Swerdlow, *Breast Cancer Res.*, 2017, **19**, 118.
6 M. J. Meegan and N. M. O'Boyle, *Pharmaceuticals*, 2019, **12**, 134.
7 D. Acharya, S. Satapathy, P. Somu, U. K. Parida and G. Mishra, *Biol. Trace Elem. Res.*, 2021, **199**, 1812–1822.
8 P. Baindara and S. M. Mandal, *Biochimie*, 2020, **177**, 164–189.
9 L. V. Spirina, A. V. Avgustinovich, S. G. Afanas'ev, O. V. Cheremisina, M. Yu. Volkov, E. L. Choynzonov, A. K. Gorbunov and E. A. Usynin, *Curr. Drug Targets*, 2020, **21**, 713–721.
10 S. Łukasiewicz, M. Czeczelewski, A. Forma, J. Baj, R. Sitarz and A. Stanisławek, *Cancers*, 2021, **13**, 4287.
11 G. Radha and M. Lopus, *Transl. Oncol.*, 2021, **14**, 101166.
12 C. Duan, M. Yu, J. Xu, B.-Y. Li, Y. Zhao and R. K. Kankala, *Biomed. Pharmacother.*, 2023, **162**, 114643.
13 A. K. McClendon and N. Osheroff, *Mutat. Res., Fundam. Mol. Mech. Mutagen.*, 2007, **623**, 83–97.
14 S. J. McKie, K. C. Neuman and A. Maxwell, *BioEssays*, 2021, **43**, 2000286.
15 V. Brázda, R. C. Laister, E. B. Jagelská and C. Arrowsmith, *BMC Mol. Biol.*, 2011, **12**, 33.
16 Y. Pommier, *Curr. Med. Chem.: Anti-Cancer Agents*, 2004, **4**, 429–434.
17 Y. Pommier, J. M. Barcelo, V. A. Rao, O. Sordet, A. G. Jobson, L. Thibaut, Z. Miao, J. A. Seiler, H. Zhang, C. Marchand, K. Agama, J. L. Nitiss and C. Redon, in *Progress in Nucleic Acid Research and Molecular Biology*, Elsevier, 2006, vol. 81, pp. 179–229.
18 A. Ray Chaudhuri, Y. Hashimoto, R. Herrador, K. J. Neelsen, D. Fachinetti, R. Bermejo, A. Cocito, V. Costanzo and M. Lopes, *Nat. Struct. Mol. Biol.*, 2012, **19**, 417–423.
19 J. J. Reynolds and G. S. Stewart, *DNA Repair*, 2013, **12**, 588–599.
20 S. Lamba and A. Roy, *Biochem. Pharmacol.*, 2022, **203**, 115158.
21 A. Dhiman, R. Sharma and R. K. Singh, *Acta Pharm. Sin. B*, 2022, **12**, 3006–3027.
22 E. Martín-Encinas, A. Selas, F. Palacios and C. Alonso, *Expert Opin. Drug Discovery*, 2022, **17**, 581–601.
23 C. Bailly, *Cytokine*, 2023, **168**, 156234.
24 F. Ye, S. Dewanjee, Y. Li, N. K. Jha, Z.-S. Chen, A. Kumar, Vishakha, T. Behl, S. K. Jha and H. Tang, *Mol. Cancer*, 2023, **22**, 105.
25 T. T. Le, M. Wu, J. H. Lee, N. Bhatt, J. T. Inman, J. M. Berger and M. D. Wang, *Nat. Chem. Biol.*, 2023, **19**, 641–650.
26 L. Oelschläger, P. Stahl, F. Kaschani, R. H. Stauber, S. K. Knauer and A. Hensel, *Cells*, 2023, **12**, 363.
27 M. Tufail, J. Cui and C. Wu, *Am. J. Cancer Res.*, 2022, **12**, 2920–2949.
28 Z. Pang, X. Dong, H. Deng, C. Wang, X. Liao, C. Liao, Y. Liao, W. Tian, J. Cheng, G. Chen, H. Yi and L. Huang, *Oncogene*, 2022, **41**, 3064–3078.
29 M. Aatif, M. A. Raza, K. Javed, S. M. Nashre-ul-Islam, M. Farhan and M. W. Alam, *Antibiotics*, 2022, **11**, 1750.
30 J. Baranwal, S. Kushwaha, S. Singh and A. Jyoti, *Curr. Phys. Chem.*, 2023, **13**, 2–19.

31 S. K. Suthar, N. S. Chundawat, G. P. Singh, J. M. Padrón and Y. K. Jhala, *Eur. J. Med. Chem. Rep.*, 2022, **5**, 100040.
32 R. S. Keri, S. S. Pandule, S. Budagumpi and B. M. Nagaraja, *Arch. Pharm.*, 2018, **351**, 1700325.
33 R. L. Lucaciu, A. C. Hangan, B. Sevastre and L. S. Oprean, *Molecules*, 2022, **27**, 6485.
34 D. Deng, Y. Yang, Y. Zou, K. Liu, C. Zhang, M. Tang, T. Yang, Y. Chen, X. Yuan, Y. Guo, S. Zhang, W. Si, B. Peng, Q. Xu, W. He, D. Xu, M. Xiang and L. Chen, *J. Med. Chem.*, 2023, **66**, 9495–9518.
35 Y. Bonakolluru, S. K. Nukala, G. Dasari, V. Badithapuram, R. Manchal and S. Bandari, *Polycyclic Aromat. Compd.*, 2023, **43**, 6319–6335.
36 X. Mu, W. Shi, L. Sun, H. Li, Z. Jiang and L. Zhang, *Molecules*, 2012, **17**, 6854–6868.
37 M.-H. Hu and J.-H. Lin, *Int. J. Biol. Macromol.*, 2023, **241**, 124548.
38 Y. Zhang, G. Li and Y. Zhao, *Bioorg. Med. Chem.*, 2023, **90**, 117337.
39 G. Dasari, S. Bandari, S. Kumar Nukala, N. Swamy Thirukovela, N. Sirassu, V. Badithapuram and R. Manchal, *ChemistrySelect*, 2022, **7**, e202200681.
40 I. Balderas-Renteria, P. Gonzalez-Barranco, A. Garcia, B. K. Banik and G. Rivera, *Curr. Med. Chem.*, 2012, **19**, 4377–4398.
41 M. A. Moga, O. G. Dimienescu, A. Bălan, L. Dima, S. I. Toma, N. F. Bîgiu and A. Blidaru, *Molecules*, 2021, **26**, 1054.
42 S. D. Undevia, F. Innocenti, J. Ramirez, L. House, A. A. Desai, L. A. Skoog, D. A. Singh, T. Karrison, H. L. Kindler and M. J. Ratain, *Eur. J. Cancer*, 2008, **44**, 1684–1692.
43 S.-H. Lee, N. Kim, S.-J. Kim, J. Song, Y.-D. Gong and S.-Y. Kim, *J. Cancer Res. Clin. Oncol.*, 2013, **139**, 1279–1294.
44 L. Marcu and I. Olver, *Curr. Clin. Pharmacol.*, 2006, **1**, 71–79.
45 Z. Wang and B. Yang, in *Polypharmacology*, Springer International Publishing, Cham, 2022, pp. 43–72.
46 I. H. El Azab, E. M. Saied, A. A. Osman, A. E. Mehana, H. A. Saad and N. A. A. Elkanzi, *Future Med. Chem.*, 2021, **13**, 1743–1766.
47 A. Kabir and A. Muth, *Pharmacol. Res.*, 2022, **176**, 106055.
48 J. Sharifi-Rad, N. Cruz-Martins, P. López-Jornet, E. P.-F. Lopez, N. Harun, B. Yeskaliyeva, A. Beyatli, O. Sytar, S. Shaheen, F. Sharopov, Y. Taheri, A. O. Docea, D. Calina and W. C. Cho, *Oxid. Med. Cell. Longevity*, 2021, **2021**, 6492346.
49 M. J. Matos, L. Santana, E. Uriarte, O. A. Abreu, E. Molina, E. G. Yordi, M. J. Matos, L. Santana, E. Uriarte, O. A. Abreu, E. Molina and E. G. Yordi, in *Phytochemicals – Isolation, Characterisation and Role in Human Health*, IntechOpen, 2015.
50 S. D. Sarker and L. Nahar, in *Progress in the Chemistry of Organic Natural Products 106*, ed. A. D. Kinghorn, H. Falk, S. Gibbons and J. Kobayashi, Springer International Publishing, Cham, 2017, pp. 241–304.
51 S. Fiorito, L. Palumbo, F. Epifano, D. Fraternale, C. Collevecchio and S. Genovese, *Biomass Convers. Biorefin.*, 2022, DOI: 10.1007/s13399-022-03309-z.
52 A. Khalid, W. Khan, K. Zia, Azizuddin, W. Ahsan, H. A. Alhazmi, A. N. Abdalla, A. Najmi, A. Khan, A. Bouyahya, Z. Ul-Haq and A. Khan, *Front. Pharmacol*, 2023, **14**, 1133809.
53 *Herbs, Shrubs and Trees of Potential Medicinal Benefits*, ed. A. Husen, CRC Press, Boca Raton, 1st edn, 2022.
54 A. Rawat and A. Vijaya Bhaskar Reddy, *Eur. J. Med. Chem. Rep.*, 2022, **5**, 100038.
55 T. Al-Warhi, A. Sabt, E. B. Elkaeed and W. M. Eldehna, *Bioorg. Chem.*, 2020, **103**, 104163.
56 J. C. Menezes and M. Diederich, *Future Med. Chem.*, 2019, **11**, 1057–1082.
57 E. M. Saied and C. Arenz, *Int. J. Mol. Sci.*, 2021, **22**, 8171.
58 E. M. Saied, S. Diederich and C. Arenz, *Chem.–Asian J.*, 2014, **9**, 2092–2094.
59 E. M. Saied, T. L.-S. Le, T. Hornemann and C. Arenz, *Bioorg. Med. Chem.*, 2018, **26**, 4047–4057.
60 E. M. Saied, S. Banhart, S. E. Bürkle, D. Heuer and C. Arenz, *Future Med. Chem.*, 2015, **7**, 1971–1980.
61 R. D. Healey, E. M. Saied, X. Cong, G. Karsai, L. Gabellier, J. Saint-Paul, E. Del Nero, S. Jeannot, M. Drapeau, S. Fontanel, D. Maurel, S. Basu, C. Leyrat, J. Golebiowski, G. Bossis, C. Bechara, T. Hornemann, C. Arenz and S. Granier, *Angew. Chem., Int. Ed.*, 2022, **61**, e202109967.
62 S. M. Khirallah, H. M. M. Ramadan, H. A. A. Aladl, N. O. Ayaz, L. A. F. Kurdi, M. Jaremko, S. Z. Alshawwa and E. M. Saied, *Pharmaceuticals*, 2022, **15**, 1576.
63 E. M. Radwan, E. Abo-Elabass, A. E. Abd El-Baky, H. A. Alshwyeh, R. A. Almaimani, G. Almaimani, I. A. A. Ibrahim, A. Albogami, M. Jaremko, S. Z. Alshawwa and E. M. Saied, *Front. Chem.*, 2023, **11**, 1231030.
64 S. M. Khirallah, H. M. M. Ramadan, A. Shawky, S. H. Qahl, R. S. Baty, N. Alqadri, A. M. Alsuhaibani, M. Jaremko, A.-H. Emwas and E. M. Saied, *Molecules*, 2022, **27**, 6271.
65 A. Olyaei, E. Feizy and A. Aghajanzadeh, *J. Heterocycl. Chem.*, 2021, **58**, 757–765.
66 G. A. Hampannavar, R. Karpoormath, M. B. Palkar, M. S. Shaikh and B. Chandrasekaran, *ACS Med. Chem. Lett.*, 2016, **7**, 686–691.
67 C. Davies, C. M. Brown, D. Westphal, J. M. Ward and V. K. Ward, *J. Virol.*, 2015, **89**, 6057–6066.
68 O. Hayes, B. Ramos, L. L. Rodríguez, A. Aguilar, T. Badía and F. O. Castro, *Anim. Reprod. Sci.*, 2005, **87**, 181–192.
69 F. Heitz, P. Harter, N. Ewald-Riegler, M. Papsdorf, S. Kommoss and A. Du Bois, *Expert Rev. Anticancer Ther.*, 2010, **10**, 1125–1136.
70 E. V. Mirkin and S. M. Mirkin, *Microbiol. Mol. Biol. Rev.*, 2007, **71**, 13–35.
71 J. Y. Kim, K.-W. Lee, S.-H. Kim, J. J. Wee, Y.-S. Kim and H. J. Lee, *Planta Med.*, 2002, **68**, 119–122.
72 H. El Hajj, B. Khalil, B. Ghandour, R. Nasr, S. Shahine, A. Ghantous, R. Abdel-Samad, A. Sinjab, H. Hasegawa, M. Jabbour, W. W. Hall, G. Zaatari, G. Dbaibo, C. Pisano,

A. Bazarbachi and N. Darwiche, *Blood*, 2014, **124**, 2072–2080.
73 C. M. Henry, E. Hollville and S. J. Martin, *Methods San Diego Calif*, 2013, **61**, 90–97.
74 B. Schutte, R. Nuydens, H. Geerts and F. Ramaekers, *J. Neurosci. Methods*, 1998, **86**, 63–69.
75 Z. Wu, L. Wu, L. Zou, M. Wang and X. Liu, *J. Chemother.*, 2023, **35**, 131–141.
76 A. Plaper, M. Golob, I. Hafner, M. Oblak, T. Šolmajer and R. Jerala, *Biochem. Biophys. Res. Commun.*, 2003, **306**, 530–536.
77 D. A. Burden and N. Osheroff, *Biochim. Biophys. Acta, Gene Struct. Expression*, 1998, **1400**, 139–154.
78 I. Laponogov, D. A. Veselkov, I. M.-T. Crevel, X.-S. Pan, L. M. Fisher and M. R. Sanderson, *Nucleic Acids Res.*, 2013, **41**, 9911–9923.
79 J. V. Walker and J. L. Nitiss, *Cancer Invest.*, 2002, **20**, 570–589.
80 J. E. Deweese and N. Osheroff, *Nucleic Acids Res.*, 2009, **37**, 738–748.
81 C. O. Okoro and T. H. Fatoki, *Int. J. Mol. Sci.*, 2023, **24**, 2532.
82 A. C. Dougherty, M. G. Hawaz, K. G. Hoang, J. Trac, J. M. Keck, C. Ayes and J. E. Deweese, *ACS Omega*, 2021, **6**, 25892–25903.
83 M. Antoniou-Kourounioti, M. Mimmack, A. Porter and C. Farr, *Int. J. Mol. Sci.*, 2019, **20**, 1238.
84 V. Singh, T. Afshan, P. Tyagi, P. K. Varadwaj and A. K. Sahoo, *Int. J. Biol. Macromol.*, 2023, **226**, 473–484.
85 H. Masuda, D. Zhang, C. Bartholomeusz, H. Doihara, G. N. Hortobagyi and N. T. Ueno, *Breast Cancer Res. Treat.*, 2012, **136**, 331–345.
86 P. Wee and Z. Wang, *Cancers*, 2017, **9**, 52.
87 R. Kshatriya, P. Shelke, S. Mali, G. Yashwantrao, A. Pratap and S. Saha, *ChemistrySelect*, 2021, **6**, 6230–6239.
88 V. R. Mishra, C. W. Ghanavatkar, S. N. Mali, H. K. Chaudhari and N. Sekar, *J. Biomol. Struct. Dyn.*, 2019, 1–14.
89 C. Kirschbaum, E. M. Saied, K. Greis, E. Mucha, S. Gewinner, W. Schöllkopf, G. Meijer, G. von Helden, B. L. J. Poad, S. J. Blanksby, C. Arenz and K. Pagel, *Angew. Chem., Int. Ed.*, 2020, **59**, 13638–13642.
90 B. A. Abdel-Wahab, H. F. Abd El-Kareem, A. Alzamami, C. A. Fahmy, B. H. Elesawy, M. Mostafa Mahmoud, A. Ghareeb, A. El Askary, H. H. Abo Nahas, N. G. M. Attallah, N. Altwaijry and E. M. Saied, *Metabolites*, 2022, **12**, 715.
91 S. Banhart, E. M. Saied, A. Martini, S. Koch, L. Aeberhard, K. Madela, C. Arenz and D. Heuer, *Antimicrob. Agents Chemother.*, 2014, **58**, 5537–5546.
92 S. Koch-Edelmann, S. Banhart, E. M. Saied, L. Rose, L. Aeberhard, M. Laue, J. Doellinger, C. Arenz and D. Heuer, *Cell. Microbiol.*, 2017, **19**, e12752.
93 L. S. Kalinichenko, C. Mühle, T. Jia, F. Anderheiden, M. Datz, A.-L. Eberle, V. Eulenburg, J. Granzow, M. Hofer, J. Hohenschild, S. E. Huber, S. Kämpf, G. Kogias, L. Lacatusu, C. Lugmair, S. M. Taku, D. Meixner, N. Tesch, M. Praetner, C. Rhein, C. Sauer, J. Scholz, F. Ulrich, F. Valenta, E. Weigand, M. Werner, N. Tay, C. J. Mc Veigh, J. Haase, A.-L. Wang, L. Abdel-Hafiz, J. P. Huston, I. Smaga, M. Frankowska, M. Filip, A. Lourdusamy, P. Kirchner, A. B. Ekici, L. M. Marx, N. P. Suresh, R. Frischknecht, A. Fejtova, E. M. Saied, C. Arenz, A. Bozec, I. Wank, S. Kreitz, A. Hess, T. Bäuerle, M. D. Ledesma, D. N. Mitroi, A. M. Miranda, T. G. Oliveira, E. Gulbins, B. Lenz, G. Schumann, J. Kornhuber and C. P. Müller, *Mol. Psychiatry*, 2021, **26**, 7403–7416.
94 T. D. de Oliveira, G. H. Ribeiro, J. Honorato, C. M. Leite, A. C. da S. Santos, E. D. Silva, V. R. A. Pereira, A. M. Plutín, M. R. Cominetti, E. E. Castellano and A. A. Batista, *J. Inorg. Biochem.*, 2022, **234**, 111906.
95 L. Huang and L. Fu, *Acta Pharm. Sin. B*, 2015, **5**, 390–401.
96 D. Samaha, H. H. Hamdo, X. Cong, F. Schumacher, S. Banhart, Ö. Aglar, H. M. Möller, D. Heuer, B. Kleuser, E. M. Saied and C. Arenz, *Chem.–Eur. J.*, 2020, **26**, 16616–16621.
97 D. I. Mohamed, D. A. Abou-Bakr, S. F. Ezzat, H. F. A. El-Kareem, H. H. A. Nahas, H. A. Saad, A. E. Mehana and E. M. Saied, *Pharmaceuticals*, 2021, **14**, 1222.
98 D. I. Mohamed, S. F. Ezzat, W. M. Elayat, O. A. El-Kharashi, H. F. A. El-Kareem, H. H. A. Nahas, B. A. Abdel-Wahab, S. Z. Alshawwa, A. Saleh, Y. A. Helmy, E. Khairy and E. M. Saied, *Pharmaceuticals*, 2022, **15**, 832.
99 S. Fathy Elhabal, M. A. El-Nabarawi, N. Abdelaal, M. F. M. Elrefai, S. A. Ghaffar, M. M. Khalifa, P. M. Mohie, D. S. Waggas, A. M. E. Hamdan, S. Z. Alshawwa, E. M. Saied, N. A. Elzohairy, T. Elnawawy, R. A. Gad, N. Elfar, H. Mohammed and M. A. Khasawneh, *Drug Deliv.*, 2023, **30**, 2241665.
100 N. Coant, J. D. Bickel, R. Rahaim, Y. Otsuka, Y.-M. Choi, R. Xu, M. Simoes, C. Cariello, C. Mao, E. M. Saied, C. Arenz, T. P. Spicer, T. D. Bannister, P. J. Tonge, M. V. Airola, L. Scampavia, Y. A. Hannun, R. C. Rizzo and J. D. Haley, *Bioorg. Chem.*, 2023, **139**, 106747.
101 D. I. Mohamed, D. Alaa El-Din Aly El-Waseef, E. S. Nabih, O. A. El-Kharashi, H. F. Abd El-Kareem, H. H. Abo Nahas, B. A. Abdel-Wahab, Y. A. Helmy, S. Z. Alshawwa and E. M. Saied, *Pharmaceutics*, 2022, **14**, 529.